

Methodological advances and theoretical experiments on the bonding regime and property design. From atoms to supra-molecules.

Report 2013-2016 Dr. Fănică Cimpoeșu

Bonding regime of d and f ion systems contained in fullerenes, complex and solid phase.

The project descended from previous concerns, applying original methodology and newly conceived treatments to the adopted case studies. An important direction is treating lanthanide ions encapsulated in fullerene systems, extending the account of f-type systems, from coordination complexes to relatively unusual and exotic species, the role of theory being to exploit the information less accessible (due to the difficulty of obtaining sizeable sample amounts for experimental handling) and perform predictions that compensate part of the missing experiment.

The bonding regime in such systems is comparable to those known from molecules or networks based on coordinative binding of lanthanide ions, as the shell f is weakly interactive and screened from external influences, feature manifest in other species, such as organometallic and fullerenes adducts, we apply methodologies of the so-called ligand-field theory (Ligand Field- LF), both at phenomenological level as well as extension to ab initio computation. To test computational methods in accounting typical LF bonding regime (small gaps in the order of 10^2 - 10^3 cm⁻¹ a in the f shell), we addressed the sub-theme of assessing and calibrating the methodology on coordinative systems containing lanthanide ions in clusters extracted of solid networks. Since such methodological developments were interesting and laborious, we prepared two papers in these different directions, one dedicated to the checking of method reproducing data for a complex series from literature and one devoted to the f ions encapsulated in solid networks, reconsidering a method of ligand field called angular model (Angular Overlap Model-AOM).¹ To this was added a work dedicated to a fullerene system with single-ion magnet behaviour,² developed in the key of ligand field modeling and prediction of properties using calculation methods and interpretation algorithms designed and tested in related works.

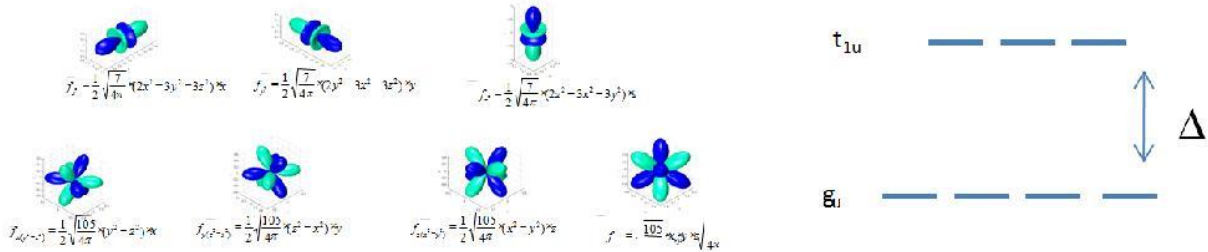
Bonding regime and stability in LnC₆₀ systems.

Systems like Ln@C₆₀ (Ln=Eu, Gd, Dy)³ are known and studied in much lesser extent than other endohedral molecules of lanthanides in fullerenes, but represent a convenient starting point in the analysis of basic properties. Using optimized geometry of the system with lutetium, observe first the geometric parameters of encapsulation, the radius of the fullerene cage, *R*, and τ index (the latter would be zero in the hypothetical situation of equality of the two types of bonds, C = C and CC, C₆₀ skeleton in icosahedral symmetry). Their relationship with the length of the link is:

$$l_{C-C} = 2R(1 - 2\tau) / \sqrt{9\gamma^2 + (1 - 2\tau)^2} \quad (1.a)$$

$$l_{C-C} = 2R(1 + \tau) / \sqrt{9\gamma^2 + (1 - 2\tau)^2}, \quad (1.b)$$

where $\gamma = (1 + \sqrt{5})/2$ is the number of gold. The LuC_{60} system consists of ionic components, Lu(III) and C_{60}^{3-} , we have $R = 3.536 \text{ \AA}$ and $\tau = -0.011$, meaning a smaller radius than the free fullerite, ($R = 3.566 \text{ \AA}$ and $\tau = -0.008$) and even than neutral fullerene ($R = 3.553 \text{ \AA}$ and $\tau = -0.013$), which certifies a stabilizing interaction. The total energy of cohesion, relative to fragment ions is high enough, -38.982 eV , the majority coming from ionic interactions (-23.304 eV) while a significant amount is due to orbital interactions (-16.256 eV), with quite low Pauli repulsion (0.578 eV).



Synopsis 1. Scheme of icosahedral field splitting of the f shell in Ln@C_{60} systems.

Although overall cohesion energy is high enough, the magnitude of the splitting in ligand field, denoted Δ in Synopsis 1 is very low. Methods of multi-configuration type (CASSCF Complete Active Space Self-Consistent Field), estimate the split of 7F term in the system TbC_{60} , a parameter $\Delta = 2.8 \text{ cm}^{-1}$, the spacing levels and t_{2u} si g_u forming representations layer f in icosahedral symmetry, I_h . Under these conditions, computational modeling is relatively risky, at the borderline of safe numerical precision, selecting then other systems for further study, which also have special properties that make them very interesting, as principle and potential application.

The theoretical approach of the ligand field, the bonding regime and magnetic anisotropy in the in endoedral fullerene $\text{DySc}_2\text{N@C}_{80}$, with single-ion magnet properties.

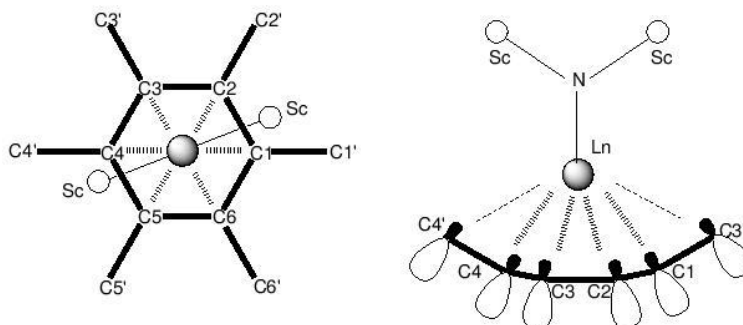
An outstanding class of systems is represented by endohedral lanthanide-fullerene compounds, the icosahedral C_{80} incorporating a triangle metal ions, triple bridged by a central nitrogen atom, different $\text{Ln}_3\text{N@C}_{80}$ systems with trivalent lanthanide ions ($\text{Ln} = \text{Gd}, \text{Tb}, \text{Dy}, \text{Ho}$) being investigated in key special magnetic properties.⁴ Heterometallic systems with this topology and mixed composition $\text{Ln}_x\text{M}_{3-x}\text{N@C}_{80}$, are also known,⁵ a challenging case being $\text{DySc}_2\text{N@C}_{80}$ having the special Single-Ion-Magnet (SIM) behavior,⁶ similar those outlined initially in mononuclear bis (phthalocyaninato) lanthanide complexes:⁷ $[\text{Pc}_2\text{Tb}]^-$, $[\text{Pc}_2\text{Dy}]^-$, $[\text{Pc}_2\text{Ho}]^-$. The SIM property is an amazing facet of the Single Molecule Magnet (SMM) paradigm,⁸ which was originally supposed to coordination compounds with large nuclearity⁹ and gradually identified in smaller systems,¹⁰ down to binuclears.¹¹ Physical chemistry of lanthanide ions in fullerenes is a new world, which is still in the early stages of exploration, showing promising prospects for a new type of molecular magnetism, challenging the fashionable topic of spintronics as future technology.¹²

Considering the DySc₂N@C₈₀ as prototype for Single Ion Magnets (SIM) based on endohedral fullerenes, we present advanced methodologies and state-of-the-art calculations for the analysis of electronic structure and its relationship with the magnetic properties. Quantum-chemical calculations results are decrypted within the ligand field (LF) concepts, in quantitative and qualitative aspects, extracting and interpreting the complete parametric sets in a heuristic picture. An important result is the characterization of magnetic anisotropy in the ground state and excited by determining the polar diagrams of magnetization functions specific to each state, giving clear visual hints about the axes of easy magnetization as response to the magnetic perturbations applied from different spatial directions. State-specific magnetization functions are derivatives with respect of magnetic field, taken to a certain eigenvalue of the calculated spectrum their maps containing full information about the corresponding axis of magnetization. The methodology is designed by exploiting data from the black box of *ab initio* spin-orbit (SO) calculations, implementing the dependence magnetic field, which allows the simulation of magnetic properties from the first principles. The calculated magnetization curves correspond to experimental measurements. The approach calculation to the properties of endohedral fullerenes is an important goal, helping to fill the deficit of experimental data for such system, due to the lack of measurable sample quantities.

Molecular geometry and general characteristics of the bonding.

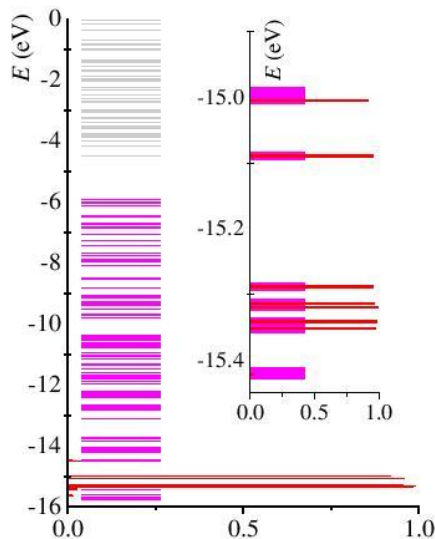
Before entering the main issue of the *ab initio* account of the specifics due to f shell in the electron structure and magnetic properties of the DySc₂N@C₈₀ system. Since the overall geometry of the molecule can be properly perceived from the following pictures, dedicated to the molecular orbitals, or from the figures of the other works^{4,5,6} we will begin with idealized image of Scheme 1. This is based on our optimized geometry. We use the LuSc₂N@C₈₀, congener to avoid complications and conceptual uncertainties related to the open f shell in classical Density Functional Theory type (DFT), on which the optimization procedures are based since otherwise the CASSCF techniques are too expensive for this purpose. Considering our goal as the semi-quantitative aspect of the mechanisms of interest (Ligand Field scheme of and magnetic anisotropy), the findings cannot be changed by small increments in bond lengths and angular parameters. In fact, it is possible to identify several local minima given the versatility reported for orientation encapsulated entity,¹³ but we confine ourselves to the current idealization as representative target. Being aware of the possible impact of so-called lanthanide contraction, i.e. the slow and steady decrease in ionic radius along the f series in the periodic table,¹⁴ is acceptable that the system can provide Lu-C underestimated with respect to Dy. However, the effect is not dramatic, since the bond lengths can vary by only 3% for isomorphous molecules with the lanthanides placed at different extremes in the series f. At the same time, fullerene is a rigid structure and we do not expect that the quite weak bonding with lanthanides (basically ionic) can modulate decisively geometric parameters of the cage itself. In other words, fullerene bonds in the unit itself constrains DySc₂N. This optimized coordinative bonds N-Lu, 2.133 Å, are noticeably shorter than the normal in lanthanide complexes. For example, diamagnetic analogue [Pc₂Lu]⁽⁻⁾ complexes of the type known as Ishikawa⁷ systems environments Lu-N distances are around 2.37-2.39 Å.¹⁵ In an approximate description, suggested in Scheme 1, the N-Ln line is

oriented towards the center of the hexagonal face of C_{80} with the C1-C6 atoms forming the corresponding first surrounding, the secondary one, drawn by C1'-C6 also capable of exerting LF perturbation on the lanthanide ion. The entire system has a C_2 symmetry, with, e.g. and Ln-C1 and Ln-C4 links equivalent. Thus, noting the symmetry independent coordination radii, the following bond lengths were obtained by DFT optimization: $R(\text{Ln-C1}) = 2.482 \text{ \AA}$, $R(\text{Ln-C2}) = 2.485 \text{ \AA}$, $R(\text{Ln-C3}) = 2.482 \text{ \AA}$, for the closest contacts and $R(\text{Ln-C1}') = 2.892 \text{ \AA}$, $R(\text{Ln-C2}') = 2.94 \text{ \AA}$, $R(\text{Ln-C3}') = 2.895 \text{ \AA}$ for the next neighbors.



Scheme 1.

Qualitatively, the system may be characterized by a strong axial character, actually due to short bond with the nitrogen atom. As the density of electrons is located on the outer surface of the fullerene, as suggested by the right side of Scheme 1, the LF effect if inner lobes on the fullerene wall towards the lanthanide, may be regarded as relatively small. The regime, in general, can be characterized as similar to organometallic compounds of lanthanides.



Synopsis 2. The diagram of MO energies from DFT calculations (BP86/TZP) for the complex $\text{LuSc}_2\text{N}@C_{80}$ including on the abscissa, histogram of f-type content for each MO. Inset: enlarged sequence containing predominantly f orbital character.

To illustrate the complications of the electronic structure treatment in f systems we present in Synopsis 2 the molecular orbital diagram of the complex $\text{LuSc}_2\text{N@C}_{80}$, putting along the abscissa the fraction f atomic orbital in each molecular orbital. It can be seen that a series of orbitals placed between -15.5 eV and -15.0 eV, well below the HOMO, located approximately at -6 eV, are almost completely f-type (with fractions showing close to unity). We identify seven atomic f-type orbitals (some in relation of quasi-degeneracy, with overlapping lines in Synopsis 2). We note the possibility of accidental degeneracy of molecular orbitals belonging to the rest of the molecule as the couple with energy levels close to -15.0 eV, one belonging lanthanide and other to the fullerene cage. There are about 100 molecular doubly occupied orbitals placed over the sequence of f typ. In the present calculation, based on a system of Lu(III) closed shell, complete configuration f^{14} , the situation is not nominal non-aufbau, but it turns to this type conceiving congeners with partially filled f shell. Such electronic structure is practically impossible to be treated in the usual methods of self-consistent single-determinant type. The unrestricted DFT can be relatively easy to use, with no convergence problems.¹⁶ A careful analysis may show that with stacks having different molecular orbitals in α and β subsystems, the convergence is achieved on the cost of their physically unreasonable separation (as energy and shape). The mechanisms behind the unrestricted- type calculations are not suitable for further exploitation in the interest of the LF analysis, even if they can provide a good description of the spin distribution in ground state.

At large molecular scale and low symmetry, non-routine approach LF-DFT becomes laborious and unsafe due to the effects of accidental degeneracy and difficulty in the assignment of the f-type molecular orbitals around the schema. For these technical reasons, we use the following the path of CASSCF calculations. We also limit at the CASSCF itself, not seeking second order perturbation procedures (PT2), in their various implementations.¹⁷ We have previously shown that for complexes of lanthanides the CASSCF calculations seem to give the same results with the PT2 after corrections. This is because this correction is designed to counter the limited choice of active space, when leaving out molecular orbitals that may be relevant to the effects investigated. This is not the case in lanthanide complexes because –surely - for a mono-nuclear complex, the LF and related physical nature of magnetism is well defined by an CASSCF (7, n) (n orbital electrons in 7) approach, which corresponds to the phenomenology of the f^n configuration for the given lanthanide ion.

Along with the system of interest,⁶ $\text{DySc}_2\text{N@C}_{80}$, we consider the $\text{TbSc}_2\text{N@C}_{80}$ congener in the current computational experiment, which is particularly convenient in interpreting LF scheme. Given the general similarity of bonding characteristics in isostructural lanthanide compounds, the conclusion from terbium system can be transferred approximately to the dysprosium case. Calculation of Tb system was achieved with a CASSCF (7,8) method, i.e. eight electrons in 7 orbitals, corresponding to the f^8 configuration, making the average over the seven states of the 7F ground term. Similarly, the Dy case assumes CASSCF(7,9) calculations, mediating the 11 states corresponding to the LF splitting of the 6H term. The data are presented in Table 1, comparing the results obtained from the use of 6-31G vs. 6-31G * bases, which are similar for each compound. This proves that the computational approach in lanthanide systems does not require high settings with rich sets based on the entire molecule, since physical description of the f shells requires only some f-AOs with reasonable atomic. In previous cases in

which the magneto-chemistry of complexes f and d-f was treated, the use of the SBKJC basis for lanthanides led to a good reproduction of experimental data,¹⁸ which allows us to believe in the reasonable performance of this basis in this case, too. Fortunately, the molecular mechanisms related to magnetism of the f shell are not so heavily dependent on the basis set, as other properties, such as molecular thermochemistry, could be.

Table 1. The result of CASSCF calculations for the lowest levels of LnDy₂@C₈₀, complexes with two basis sets (6-31G and 6-31G*) on the fullerene moiety. The seven Ln = Tb levels correspond to the case of LF splitting of the ⁷F multiplet. The eleven states in Ln = Dy case are related to the term ⁶H.

Ln	Basis set on C	Tb	Tb	Dy	Dy
		6-31G	6-31G*	6-31G	6-31G*
1		0.0	0.0	0.0	0.0
2		91.5	85.7	2.0	1.8
3		454.5	467.4	787.4	797.6
4		508.1	520.0	792.2	801.8
5		1219.1	1260.1	919.3	952.7
6		1239.4	1263.7	978.1	1007.6
7		1285.9	1306.1	1113.3	1147.2
8				1138.5	1172.2
9				1242.1	1269.5
10				1350.9	1378.0
11				1363.9	1388.4

Full ligand field modeling is done by analyzing the matrix of ab initio CASSCF, by fitting it to the phenomenological LF ligand field, in its classical form:

$$\hat{H}_{LF} = \sum_{k=2,4,6} \sum_{q>0} \sqrt{\frac{4\pi}{2k+1}} \left[B_q^k (Y_{k,q} + (-1)^q Y_{k,-q}) + i B_{-q}^k (Y_{k,-q} - (-1)^q Y_{k,q}) \right] + \sum_{k=2,4,6} \sqrt{\frac{4\pi}{2k+1}} B_0^k Y_{k,0} \quad (2)$$

Since the definition of B_q^k parameters may vary by particular conventions (e.g. parameterization Wybourne)¹⁹ we converted the set into so-called Stevens normalized parameters,^{20:}

$$B_q^k = \lambda_{k,q} A_{k,q} \langle r^k \rangle, \quad (3)$$

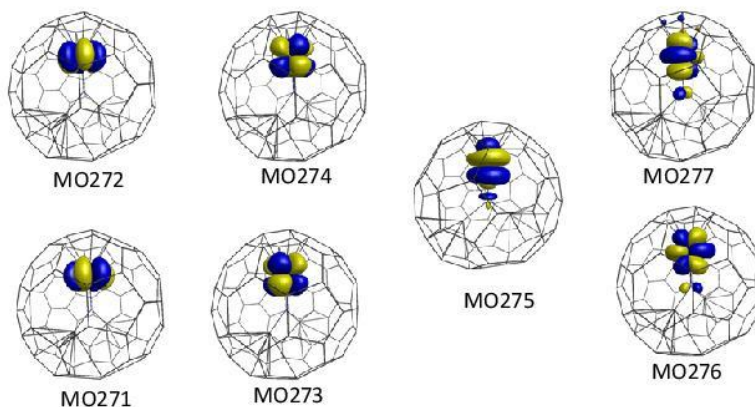
by rescaling factors λ_{kq} (found in Table 2.2. in the monograph of Newman).²¹

Data processed from ab initio Hamiltonian blocks (size 7×7 for Terbium corresponding period ⁷F, and 21×21 for dysprosium, containing the ⁶H si ⁶F terms) fitted to analytical LF expressions are presented in Table 2.

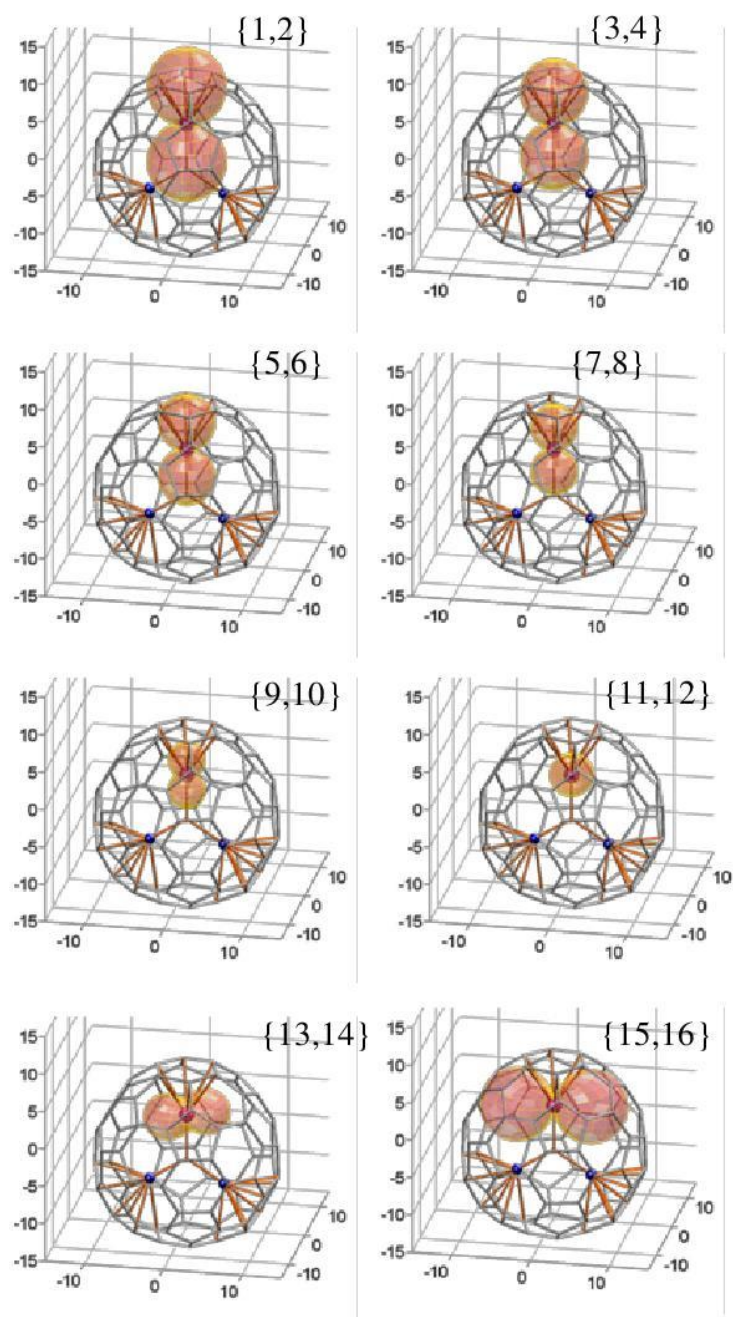
Table 2. The $A_{k,q}\langle r^k \rangle$ parameters (in cm^{-1}) resulting from the LF analysis of the ab initio computed data for $\text{LnSc}_2\text{NC}_{80}$ ($\text{Ln}=\text{Tb}, \text{Dy}$).

Ln	Tb	Tb	Dy	Dy
Basis set on C	631-G	631-G*	631-G	631-G*
$A_{2,-2}\langle r^2 \rangle$	-40.5	-45.2	0.0	0.0
$A_{2,0}\langle r^2 \rangle$	1065.0	1095.1	1321.0	1346.0
$A_{2,2}\langle r^2 \rangle$	-164.4	-126.1	-148.1	-149.9
$A_{4,-4}\langle r^4 \rangle$	-38.5	-45.0	0.0	0.0
$A_{4,-2}\langle r^4 \rangle$	7.5	11.1	-0.9	-1.3
$A_{4,0}\langle r^4 \rangle$	86.3	90.1	88.8	91.8
$A_{4,2}\langle r^4 \rangle$	-18.9	11.7	12.0	14.0
$A_{4,4}\langle r^4 \rangle$	25.0	22.9	19.8	17.9
$A_{6,-6}\langle r^6 \rangle$	123.3	114.4	112.3	103.2
$A_{6,-4}\langle r^6 \rangle$	78.9	87.8	83.1	81.0
$A_{6,-2}\langle r^6 \rangle$	-31.4	-29.1	-38.9	-37.8
$A_{6,0}\langle r^6 \rangle$	-46.2	-44.1	-46.1	-43.7
$A_{6,2}\langle r^6 \rangle$	96.6	106.5	109.4	108.4
$A_{6,4}\langle r^6 \rangle$	-48.4	-44.0	-41.4	-40.5
$A_{6,6}\langle r^6 \rangle$	19.4	17.9	16.4	14.9

It is interesting to inspect the canonical molecular orbitals of molecule $\text{DySc}_2\text{@C}_{80}$. The shape and the order is similar in the terbium congener, the qualitative appearance being also independent of the basis set. It is noted that the MO shapes are similar to the f pure AOs in axial symmetry, with the approximate ordering $\{xyz, z(x^2-y^2)\}$, $\{x(x^2-3y^2), y(3x^2-y^2)\}$, z^3 , $\{xz^2, yz^2\}$.



Synopsis 3. Canonical molecular orbital calculation derived from CASSCF(7,9) calculation on the $\text{DySc}_2\text{@C}_{80}$ system. The labels correspond to the order number in molecular orbital list.



Synopsis 4. Polar maps of state specific magnetization functions for the LF split components of the $J = 15/2$, multiplet resulted from ab initio calculations. The 3D frame in each panel corresponds to the M_x , M_y , M_z multiplet of magnetization (from $-15 \mu_B$ to $+15 \mu_B$ on each axis).

We will focus our attention again on the DySc₂NC₈₀ system. A very suggestive way to discuss the anisotropy consists in generating polar maps of derivatives of eigenvalues of ab initio CASSCF-SO Hamiltonian as function of the magnetic field:

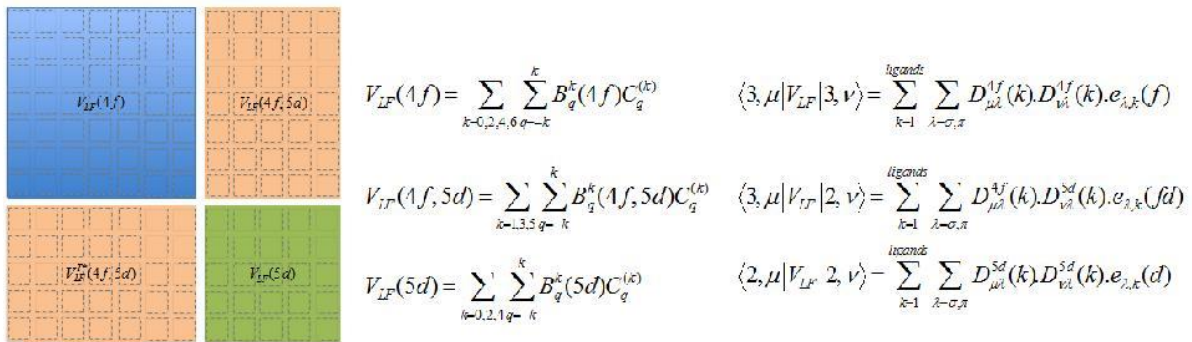
$$M_i(\theta, \varphi) = -(dE_i / dB)_{\theta, \varphi} \quad (4)$$

state called specific magnetization functions. Macroscopic magnetization is a statistic on such components. Polar maps for the states of the discussed system are represented in the Synopsis 4. Maxima extensions of the magnetization lobes of states for couples from {1, 2} to {9, 10}, correspond respectively to the {9.95, 8.52, 7.20, 5.88, 4.36} μ_B values. These sizes are close to the series {10.00, 8.67, 7.33, 6.00, 4.67} μ_B obtained by estimating with the ideal $g_J = 4/3$ factor and projections $J_z = \{\pm 2.15, \pm 13 / 2, \pm 2.11, \pm 2.9, \pm 7/2\}$. A non-trivial result is that the anisotropy of higher levels deviates from the axial model and show lobes approximately located within the Sc₂N plane. In the case of the upper levels, J_z is no longer a good quantum number, the polar maps of magnetization showing axes oriented in other plane (x in xz).

Non-covalent spin interactions in endohedral systems with encapsulated ion.

Electronic structure, magnetism and spin coupling in Ln₂@C₈₀ and related systems Ln Ln₂@C₇₉N. Calculations and interpretations. Optical and magnetic properties.

A preliminary methodological approach to the problem of endohedral metal-fullerene systems consisted elaborating a model of the ligand field model extended to more electronic shells. This method, published recently,¹ is outlined in Synopsis 5. This development is needed, conceptually and technically, to describe the surrounding with high polar strain felt by asymmetrically encapsulated metal ions. The traditional methods of the ligand field are devoted to a single shell of d type for complexes of transition metal ions,²² or f type for lanthanide systems.²³ In each case the description is tacitly affected by the so-called holohedrization effect.²⁴



$$V_{LF}(4f) = \sum_{k=0,2,4,6} \sum_{q=k} B_q^k(4f) C_q^{(k)} \quad \langle 3, \mu | V_{LF} | 3, \nu \rangle = \sum_{k=1}^{ligands} \sum_{\lambda=\sigma, \pi} D_{\mu\lambda}^{4f}(k) D_{\nu\lambda}^{4f}(k) e_{\lambda,k}(f)$$

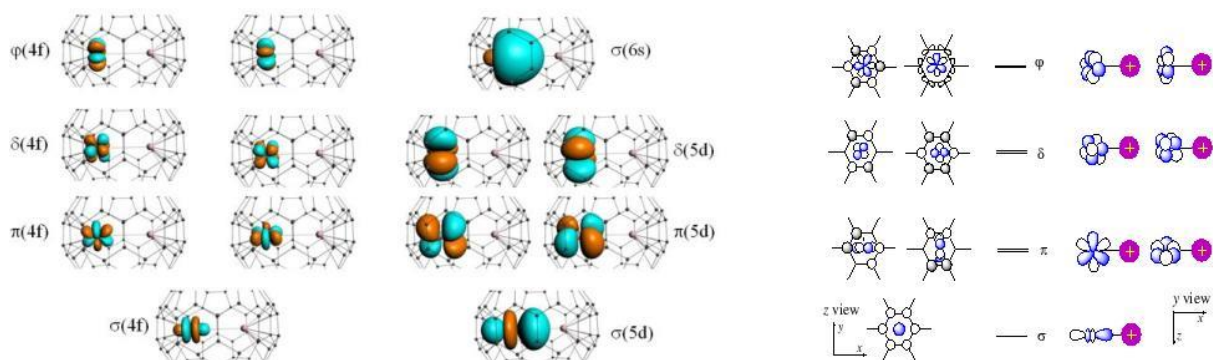
$$V_{LF}(4f, 5d) = \sum_{k=1,3,5} \sum_{q=k} B_q^k(4f, 5d) C_q^{(k)} \quad \langle 3, \mu | V_{LF} | 2, \nu \rangle = \sum_{k=1}^{ligands} \sum_{\lambda=\sigma, \pi} D_{\mu\lambda}^{4f}(k) D_{\nu\lambda}^{5d}(k) e_{\lambda,k}(fd)$$

$$V_{LF}(5d) = \sum_{k=1,2,4} \sum_{q=k} B_q^k(5d) C_q^{(k)} \quad \langle 2, \mu | V_{LF} | 2, \nu \rangle = \sum_{k=1}^{ligands} \sum_{\lambda=\sigma, \pi} D_{\mu\lambda}^{5d}(k) D_{\nu\lambda}^{5d}(k) e_{\lambda,k}(d)$$

Synopsis 5. Schematic representation of the ligand field corresponding matrix model dual-layer extended 4f and 5d orbital base.

Namely, whatever the inversion symmetry of a given orbital set is, odd or even, (e.g. labeled g for d shell, or u symmetry for f) d - d or f - f blocks will represent only symmetry of g type, due to well known rules of multiplication: $g \times g = g$, $u \times u = g$. In the paper published in the previous stage,²⁵ dedicated system $\text{DySc}_2\text{N}@C_{80}$ as prototype Single Ion Magnet (SIM) fullerene, we highlighted the limitations imposed by the holohedrization effect when one considers only f -type ligand field. Therefore, the model sketched in Synopsis 5 developed in conjunction the actual stage objectives is needed to overcome these limitations.

Calculations applied to selected systems,²⁶ $\text{Gd}_2@C_{80}$ and $\text{Gd}_2@C_{79}\text{N}$, used the Frozen Density Embedding method that builds a perturbation consistent with the purposes of the ligand field theories. The results are illustrated in Synopsis 6, by corresponding Kohn-Sham orbitals and the qualitative interaction scheme for a metal center, influenced by its close companion in dimer, in fullerenes.



Synopsis 6. Orbitals from Frozen Density Embedding (FDE) calculations for a Gd(III) center, in Gd_2C_{80} and $\text{Gd}_2\text{C}_{79}\text{N}$ (left panel) and qualitative interaction diagram (right panel).

Considering the fit by ligand field modeling, we take the above mentioned orbital energies, relative to the lowest value, expressed in wavenumber units: $\varepsilon(4f) = \{0, 137.1, 161.3, 467.8, 484.0, 903.4, 927.6\} \text{ cm}^{-1}$, $\varepsilon(5d) = \{82870.1, 90153.7, 90387.6, 93565.6, 93654.3\} \text{ cm}^{-1}$ and $\varepsilon(6s) = 103519.0 \text{ cm}^{-1}$. For the f suite, is clearly observed the series of non-degenerate lowest level, followed by quasi-degenerate couples related to the discussed $\sigma < \pi < \delta < \varphi$ ordering. The similar $\sigma < \pi < \delta$ regularity is observed also for the d set. Relative to the lowest d -type level, the energies of the set are: $0, 7283.6, 7517.5, 10695.5, 10784.2 \text{ cm}^{-1}$. One notes the magnitude of the spacing, in the range of hundreds reciprocal centimeters for the f set, while a total gap of about ten thousand wavenumbers for the ligand field split of d shell, in concordance with general expectation for f and d ligand field cases. The matrix of eigenvectors, energy is transformed into a matrix made based on actual atomic orbitalelor f , d and s . The ligand field parameters fitted for the $\text{Gd}_2@C_{79}\text{N}$ system are presented in Table 3.

The icosahedral isomer of the C_{80} has a fourfold degenerate Highest Occupied Molecular Orbital (HOMO) g_g , occupied with only one pair of electrons: $(g_g)_2^2$. This situation is not convenient for

the neutral species, implying instability and distortions. The closed shell structure, $(g_g)^8$, is achieved for the highly negative charged C_{80}^{6-} ion, which becomes then favourable for hosting positive ions, the ensemble being proven as stable. The $C_{79}N$ has the same skeleton as the icosahedral C_{80} , but the symmetry is lowered to C_s point group, having no orbital sets with large degeneracy. However, in terms of quasi-degenerate situation, the trend for acquiring negative charges is kept, the closed shell configuration being achieved at the five negative anion, $(C_{79}N)^{5-}$. In $Ln_2@C_{79}N$ compounds, the cage formally charged with six electrons, $(C_{79}N)^{6-}$, carries an unpaired electron.

Table 3. The ligand field parameters fitting the FDE calculations representing one Gd(III) site in $Gd_2@C_{79}N$ (while the other lanthanide ion and the fullerene cage are taken as frozen density fragments). All values are in cm^{-1} .

(ab)	(ff)	(dd)	(ss)	(fd)	(fs)	(ds)
$B_0^0(ab)$	454.8	91008.6	99006.0	0.0	0.0	0.0
$B_0^1(ab)$	0.0	0.0	0.0	2937.1	0.0	0.0
$B_0^2(ab)$	-1420.9	-4578.2	0.0	0.0	0	-19096.9
$B_0^3(ab)$	0.0	0.0	0.0	853.7	1401.0	0
$B_0^4(ab)$	-156.6	-8240.9	0.0	0.0	0.0	0.0
$B_0^5(ab)$	0.0	0.0	0.0	-82.2	0.0	0.0
$B_0^6(ab)$	-46.2	0.0	0.0	-82.2	0.0	0.0

Then, the $Ln_2@C_{79}N$ system can be formally considered as a symmetric trinuclear MXM, with M corresponding to the Gd(III) ions ($S_M=7/2$) and X the spin originating from the cage, with $S_X=1/2$. In turn, the $Ln_2@C_{80}$ is, from the magnetic point of view, a genuine dimer, with the fullerene possibly influencing the magnetic orbitals, but not entering in the spin count. For $Ln_2@C_{79}N$ formulated as a trimer, Hamiltonian is:

$$\hat{H}_{MXM} = -2J_{MM}\hat{S}_{M(1)} \cdot \hat{S}_{M(2)} - 2J_{MX}\hat{S}_X \cdot \hat{S}_{M(1)} - 2J_{MX}\hat{S}_X \cdot \hat{S}_{M(2)} \quad (5)$$

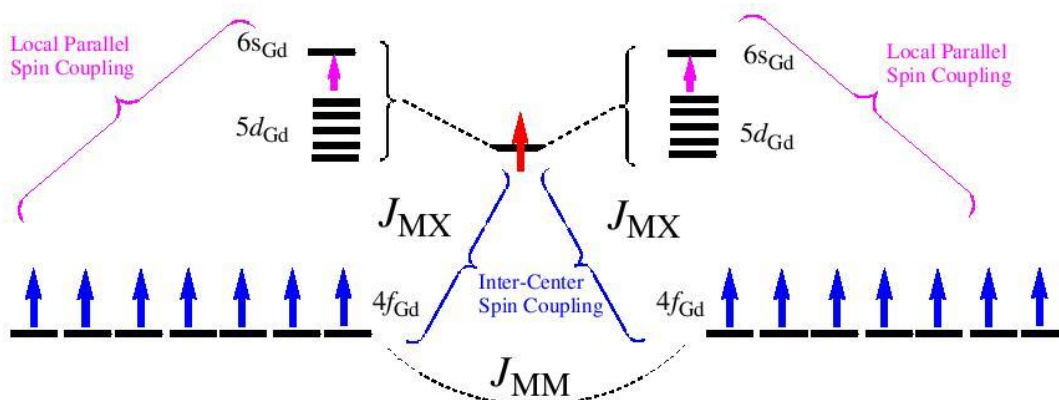
with energies:

$$E_{MXM}(S_{MXM}, S_{MM}) = -J_{MX}S_{MXM}(S_{MXM}+1) + (J_{MX} - J_{MM})S_{MM}(S_{MM}+1). \quad (6)$$

407.3, 814.5, 1220.2 cm^{-1} . One observes the regularity of equal spacing of the energy levels, or, in other words, the approximate 1:2:3 ratio for the presented values. This is in line with the predominance of a large J_{MX} value over a small J_{MM} coupling. More exactly, the outlined states

are in line with the following levels: $E_{MXM}(15/2,7)=0$, $E_{MXM}(13/2,6)=J_{MX}+14J_{MM}$, $E_{MXM}(11/2,6)=2J_{MX}+26J_{MM}$, $E_{MXM}(9/2,6)=3J_{MX}+36J_{MM}$.

The presented sequence clearly illustrates the pattern of the exchange, based on a large J_{MX} ferromagnetic coupling, the fitted values being $J_{MX}=407.11 \text{ cm}^{-1}$ and $J_{MM}=0.011 \text{ cm}^{-1}$. The calculation on the $\text{Gd}_2@C_{80}$ yielded $J_{MM}=0.027 \text{ cm}^{-1}$, namely a weak ferromagnetic coupling comparable to those found in the $\text{Gd}_2@C_{79}\text{N}$ heterofullerene case. The mechanism of interaction in $\text{Gd}_2@C_{79}\text{N}$ is represented in a simplified manner in Scheme 2. The fraction of half a electron of 5d type assigned to each Gd (III) core has the spin aligned parallel with the seven unpaired electrons of shell f. This effect makes the electron placed in the superior 5d orbital to engage effectively ferromagnetic with both lanthanide centers.



Scheme 2.

In the following we will switch the analysis tools, meeting the terms of Broken Symmetry Density Functional Theory (BS-DFT).²⁷ As well known, the DFT is a single determinant method, while the magnetic states are, in general, multi-configuration objects. Although, the DFT can approach the molecular magnetism by appropriate numeric experiments, the BS states having not a physical reality, but being appropriately tailored to reveal information on the spin Hamiltonian parameters. In the crudest approximation, the BS states are interpretable with the Ising-type Hamiltonian, replacing the scalar product of spin operators with numeric multiplication of the local spin projections, $S_{z(A)}S_{z(B)}$. The Ising terms are actually the diagonal of a full Heisenberg Hamiltonian. In the BS phenomenology, the total switch of the spin at one centre implies that only the $+S_A S_B$ or $-S_A S_B$ (positive or negative) amounts are allowed. The Ising interpretation would be valid if the BS calculation will be based on restricted-type orbitals, with the same space contours for corresponding α and β sets. However, the BS calculations are conceived and carried out in unrestricted spin schemes. In such circumstances, one may conceive the $|\langle \hat{S}_A \cdot \hat{S}_B \rangle|$ expectation value as parameter entering with plus or minus signs, $\pm |\langle \hat{S}_A \cdot \hat{S}_B \rangle|$, in the formulation of the expectation value of the spin Hamiltonian, if the given configuration records, respectively, identical or opposite spin polarities on the A and B centres. For the MXM trimer formulation of the di-lanthanido-heterofullerene case, there are three

distinct broken symmetry configurations: $\Omega(\text{HS})=\text{M}(1)^+\text{X}^+\text{M}(2)^+$, $\Omega(\text{BS1})=\text{M}(1)^+\text{X}^-\text{M}(2)^+$, and $\Omega(\text{BS2})=\text{M}(1)^+\text{X}^+\text{M}(2)^-$. The expectation value from a BS configuration Ω is ascribed as follows:

$$\langle \Omega | \hat{H}_{\text{MXM}} | \Omega \rangle = E_0 - 2\sigma_{\text{M}(1)}^\Omega \sigma_{\text{M}(2)}^\Omega J_{\text{MM}} \left| \langle \hat{S}_{\text{M}(1)} \cdot \hat{S}_{\text{M}(2)} \rangle \right| - 2\sigma_{\text{X}}^\Omega \sigma_{\text{M}(1)}^\Omega J_{\text{MX}} \left| \langle \hat{S}_{\text{X}} \cdot \hat{S}_{\text{M}} \rangle \right| - 2\sigma_{\text{X}}^\Omega \sigma_{\text{M}(2)}^\Omega J_{\text{MX}} \left| \langle \hat{S}_{\text{X}} \cdot \hat{S}_{\text{M}} \rangle \right|, \quad (7)$$

where the σ coefficients are ± 1 factors with respect to spin up or spin down population of the given centre, in the considered configuration. In the HS configuration, we have all the coefficients equal to unity $\frac{\text{HS}}{\text{M}(1)} = 1$, $\frac{\text{HS}}{\text{X}} = 1$, $\frac{\text{HS}}{\text{M}(2)} = 1$. For the BS1 configuration, the spin on the X subsystem is flipped, having therefore: $\frac{\text{BS1}}{\text{M}(1)} = 1$, $\frac{\text{BS1}}{\text{X}} = -1$, $\frac{\text{BS1}}{\text{M}(2)} = 1$. The BS2 case flips the spin on the second metal ion: $\frac{\text{BS2}}{\text{M}(1)} = 1$, $\frac{\text{BS2}}{\text{X}} = 1$, $\frac{\text{BS2}}{\text{M}(2)} = -1$. In this case, the relative trimer BS energies are:

$$\Delta E_{\text{BS1}} = E_{\text{BS1}} - E_{\text{HS}} = 8J_{\text{MX}} \left| \langle \hat{S}_{\text{X}} \cdot \hat{S}_{\text{M}} \rangle \right|, \quad (8a)$$

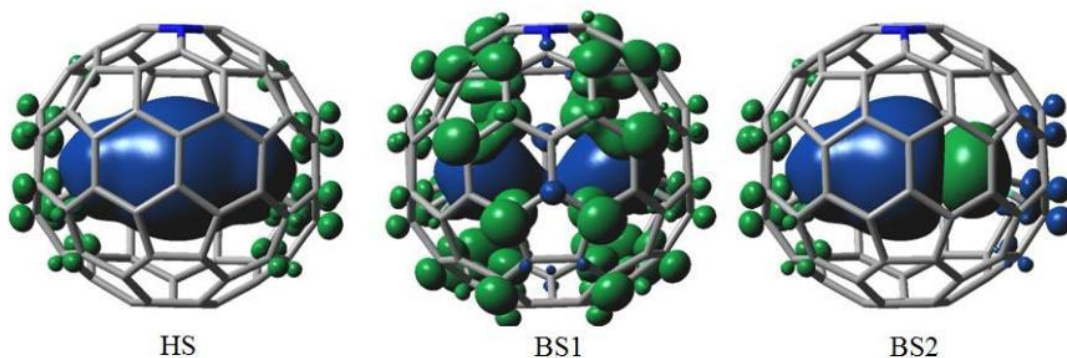
$$\Delta E_{\text{BS2}} = E_{\text{BS2}} - E_{\text{HS}} = 4J_{\text{MM}} \left| \langle \hat{S}_{\text{M}(1)} \cdot \hat{S}_{\text{M}(2)} \rangle \right| + 4J_{\text{MX}} \left| \langle \hat{S}_{\text{X}} \cdot \hat{S}_{\text{M}} \rangle \right|. \quad (8b)$$

In similarity with energy treatment, relative differences in mean squared spin operator are:

$$\Delta \langle S^2 \rangle_{\text{BS1}} = -8 \left| \langle \hat{S}_{\text{X}} \cdot \hat{S}_{\text{M}} \rangle \right|, \quad (9a)$$

$$\Delta \langle S^2 \rangle_{\text{BS2}} = -4 \left| \langle \hat{S}_{\text{M}(1)} \cdot \hat{S}_{\text{M}(2)} \rangle \right| - 4 \left| \langle \hat{S}_{\text{X}} \cdot \hat{S}_{\text{M}} \rangle \right|. \quad (9b)$$

The BS-DFT treatment (with BP86 functional and the previously mentioned basis sets) gives the following energy gaps: $\Delta E_{\text{BS1}} = 6113.24 \text{ cm}^{-1}$ and $\Delta E_{\text{BS2}} = 1927.64 \text{ cm}^{-1}$. The unrestricted DFT calculation prints out the expectation values for the $\langle S^2 \rangle$, which for the HS, BS1 and BS2 cases are 63.82, 49.79, 7.8, respectively. Differences of -14.93 and -56.33 correspond to Eqs. (9a) and (9b). These relative values determine the parameters $\left| \langle \hat{S}_{\text{X}} \cdot \hat{S}_{\text{M}} \rangle \right| = 1.87$ and $\left| \langle \hat{S}_{\text{M}(1)} \cdot \hat{S}_{\text{M}(2)} \rangle \right| = 12.22$. The fit to BS computations yields the exchange coupling parameters: $J_{\text{MX}} = 409.60 \text{ cm}^{-1}$ and $J_{\text{MM}} = -23.11 \text{ cm}^{-1}$. One notes the remarkable closeness of J_{MX} value to those computed in the CASSCF treatment. In turn, J_{MM} is negative and possibly slightly overestimated. This discrepancy does not affect the qualitative and semi-quantitative picture, common to both approaches, namely a dominating ferromagnetic MX type of coupling, overriding the direct MM interaction, irrespective of its ferromagnetic or antiferromagnetic nature.



Synopsis 7. Spin polarization in Broken Symmetry configurations generated for $Gd_2@C_{79}N$.

The experimental information for estimation of these parameters is very limited,²⁶ given the trace amounts of sample that can be produced. To calibrate the methodology verifies its ability to predict realistic data, two other works were produced as a preamble related to this objective.^{28,29}

The artificial dimer moiety $(Gd_2)^{6+}$ from the Gd^{3+} ions is unstable, as expected, with positive bonding energy, 0.4906 Hartree. The electrostatic part, 1.2390 Hartree, is very close to the point charge estimation, considering the 3.844 Å internuclear distance. The Pauli repulsion is very small, about 0.0002 Hartree, in accordance to the point that lanthanides are bodies with electron density well confined around the nuclei, with small propensity for long-range interactions, except the ionic effects. However, surprisingly, the orbital stabilization is sizeable, about -0.7486 Hartree. The orbital stabilization can be assigned merely to polarization effects located on the fragment, rather than to the direct overlap of the *f*-type orbitals. The $Gd_2@C_{80}$ formed from two Gd^{3+} fragments and the C_{80}^{6-} negative cage shows a net bonding stabilization of -4.7976 Hartree. The Pauli repulsion is 0.4627 Hartree, entirely coming from the interference of lanthanide ionic bodies with the inner walls of the cluster, once previously showed that the dimer had this component almost negligible. The net orbital stabilization, -3.1043 Hartree, is due also to the weak covalence established with the fullerene, by each lanthanide ion.

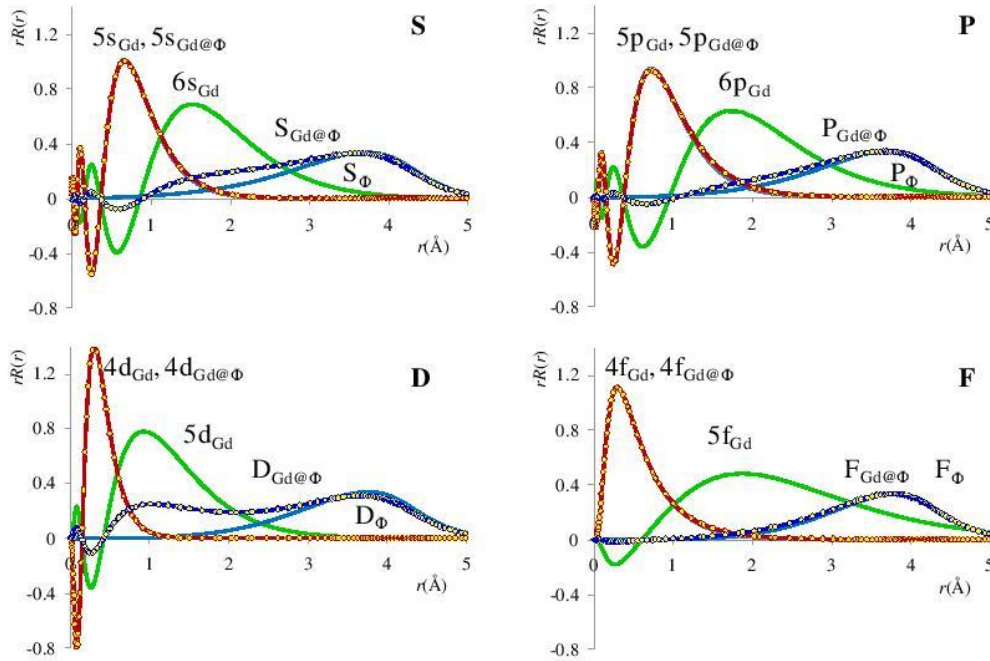
This methodology of analysis was discussed in review mode in a chapter published in the series Structure and Bonding.³⁰

Another way to highlight the dynamic effects in the formation of endohedral metal complexes is an idealized model of atom-in-the sphere with the wave functions produced in alternative manner, solving differential equations of the Hamiltonian based on numerical treatment of the local density approximation and spherical symmetry of the problem. The key is to replace the kinetic differential by a finite difference operator, resulting in a matrix system tridiagonal, having the lines defined as follows:

$$\left(\begin{array}{ccc} \frac{-1}{(r_{k+1}-r_{k-1})(r_k-r_{k-1})}, & \frac{1}{(r_{k+1}-r_k)(r_k-r_{k-1})} + V(r_k) + \frac{1}{2} \frac{l(l+1)}{r_k^2}, & \frac{-1}{(r_{k+1}-r_{k-1})(r_{k+1}-r_k)} \end{array} \right) \cdot \begin{pmatrix} r_{k-1}R_{k-1} \\ r_k R_k \\ r_{k+1}R_{k+1} \end{pmatrix} = E_l \cdot (r_k R_k) \quad (10)$$

This can be formulated as an eigenvalues-eigenvectors problem, leading directly to the radial dependence for a set of eigenfunctions, the vector set having the same dimensionality as the number of defined grid points.

The Synopsis 8 shows the analysis on orbital components with s, p, d and f symmetries. The series of panels show that the last occupied orbitals in each set (5s_{Gd}, 5p_{Gd}, 4d_{Gd}, 4f_{Gd}), represented by continuous line, are practically superposable on the points representing a corresponding wavefunction in the Gd@Φ complex (5s_{Gd@Φ}, 5p_{Gd@Φ}, 4d_{Gd@Φ}, 4f_{Gd@Φ}).



Synopsis 8. Comparison of radial deformation of the radial parts of lanthanide components in interaction with the sphere of inclusion on various channels of orbital symmetry.

The first virtuals of the lanthanide ion ($6s_{\text{Gd}}$, $6p_{\text{Gd}}$, $5d_{\text{Gd}}$, $5f_{\text{Gd}}$) are shown with light green line. The $\text{Gd}@Φ$ assembly shows the built of series of functions occupied with electrons formally originating from the cage, having the appearance of hybrids between the function on the empty sphere and the corresponding lanthanide virtuals. This trend is most visible for the d-case (see the $D_{\text{Gd}@Φ}$ profile showing maxima parallel to both $5d_{\text{Gd}}$ and $D_Φ$ lines), sustaining the above statements about the role of 5d orbitals in the bonding scheme of the lanthanide complexes. In turn, the f orbitals show almost no trace of such a deformation effect, the $F_{\text{Gd}@Φ}$ dotted profile being coincident to $F_Φ$, with no hybridization to $5f_{\text{Gd}}$. This result is consistent with the above considerations on the f shell rigidity against changes from outer perturbations.

Non-covalent interactions in the physical chemistry of supra-molecular assemblies of endohedral encapsulation type.

Non-covalent interactions in Ng@C₆₀ (Ng=Ar, Kr) endohedral systems. Bonding, vibration spectral manifestations, aromaticity and related effects.

The Density Functional Theory (DFT) is, indisputably, the most popular approach to the electron structure of matter, from molecules to solid state systems, the revolution of computing facilities, hardware and software, continuously ascending in the last two decades, opening the way for multiple practical applications in chemistry and physics. Several Pleiades of approximations for the key ingredient of the theory, the exchange-correlation functional, identified recipes for putting in practice the conceptual promises and premises of the early Hohenberg-Kohn³¹ and Kohn-Sham³² algorithm.

A drawback of the practical DFT is the wrong long range behaviour of most of genuine functionals, that impinges upon the estimation of intermolecular forces.^{33, 34} The limitation does not belong, therefore, to the conceptual level of DFT, but to its practical approximations. Given the actual interest for the supramolecular chemistry and nano-scale materials and devices, the mentioned limitation seems a serious shade on the DFT territory, the attempts in solving this problem getting a growing impetus in the last years.

Thus, aside to the already large zoo of functionals, many varieties aiming to alleviate the account of long range interaction appeared. A methodological route consists in the splitting of short-range (SR) and long-range (LR) Coulomb inter-electronic interaction, so that at large distances from the atomic nuclei, regions where the electron densities decay exponentially, the correct $-1/r$ pattern is approached. Several authors and groups (Savin,³⁵ Tsuneda and Hirao^{36,37}) discussed the principles of this branch of theory, as well as the implementation in computer codes. These approaches have the advent to follow a first principle rationales. At the same time, given the level of subtle effects acting in the low energy range, one may inquire whether the mechanisms needed to account van der Waals type of forces are really incorporated in existing functionals, even after amending their wrong asymptotic trends. Another approach, a more Gordian knot cutting style, consists in the “enforced” add of dispersion terms, a posteriori to a DFT calculation, as is the case of parameterizations advanced by Grimme³⁸. This should, in principle, supersede the consequences long range defects and, besides, make sure that a van der Waals behaviour is inserted the voids of inter-molecular space. The drawback of the dispersion

correction-based approaches may be considered in its empirical appearance, in spite of the fact that the needed interatomic parameters are built, as much as possible, on first principle grounds.

The existing amendments of long range behavior and inclusion of dispersion terms briefly described above, benefited from consistent and extensive debates and assessments on various benchmarks of prototypical intermolecular assemblies. Here, we propose a new particular test, taking the endohedral fullerenes with a noble gas in the symmetry center, Ng@C₆₀, where Ng represents the Ar and Kr atoms. This choice puts the evaluation of the van der Waals effects in a firm test: at one hand, there are many summed van der Waals interactions to be accounted, namely sixty noble gas atom –carbon contacts, the relatively large amount of total interaction ensuring a good resolution of the effect, in the numeric respects. On the other hand, the attempt to evaluate the interaction potential in the standard manner, namely scanning the distance between the interacting molecules faces a severe technical problem. Thus, in order to search for the distance dependence of the sixty Ng-C contacts, one has to enforce thirty C=C double bonds and sixty C-C simple bonds, whose covalent energy supersedes by about six order of magnitude the non-covalent contributions. In normal situations of van der Waals energy computations the moving pieces are molecules whose inner structure does not change in the process of tuning the intermolecular distances, say in associations like the Ar-Ar noble gas weakly bonded diatomic, or the Ar-C₆H₆ and C₆H₆ - C₆H₆ prototypical complexes. The molecular energies are placed in the range of molecules of moderate size, in the range of 10²-10³ Hartree, while the van der Waals interaction are at about 10⁻³ scale. When the molecular energy part itself is strongly affected by the scan aimed to search the van der Waals effects, like in the case of varying the radius of Ar@C₆₀ case, it appears a new type of numeric problem in evaluating the van der Waals curve: the obtaining of a small variation as difference of larger amounts variations. The situation is, somewhat contrasting with the simpler example of the Ar-C₆H₆ (taken in the pyramidal geometry, with C_{6v} point group) where the separation of the entities does not drastically affect their electron structure, the small variation being then evaluated as difference of larger, but not strongly varying quantities. The Ng-C potential cannot be explored at large separation of van der Waals curve since this imply the dissociation of the C₆₀ cage, entering serious problems of convergence about the meaning of the nature of the wavefunction itself. The carbon atoms have orbitaly degenerate triplet groundstates, ³P, and besides, a collection of weakly interacting atoms,

as happens at large inflation of the former fullerene cages is, in fact, a quasi-degenerate system, meeting situations that violate the limits validity of DFT, confined to nondegenerate groundstates.

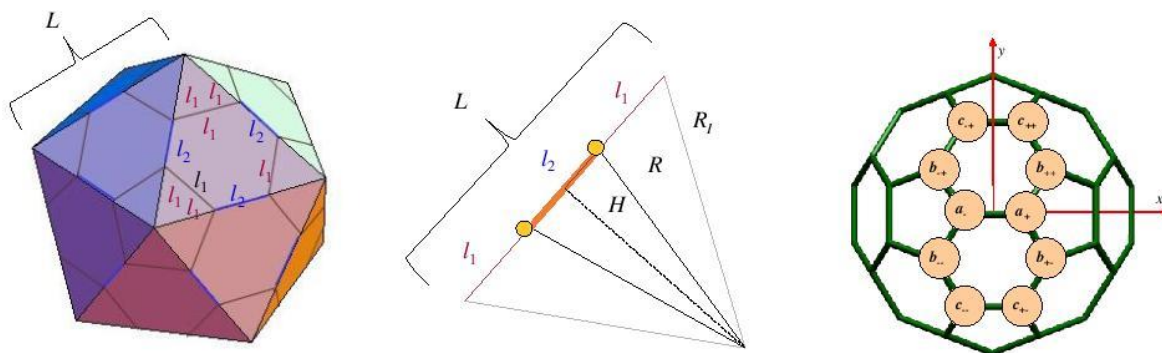
It seems then that only infinitesimal scans of Ng-C distances, or, equivalently, the radius of endohedral fullerene, around the equilibrium geometry, are allowed, in order to investigate the van der Waals curve. In this way one may find information about the local curvature of the van der Waals potential. This fact brings the idea to focus the study on the vibrational properties of endohedral fullerene, since the curvature of the potential energy curve is related with the force constant and the frequency on the corresponding coordinate.

A useful preamble to the following modelling is the definition of the molecular geometry of C_{60} cage. In this respect, its parentage from icosahedron is considered, the fullerene polyhedron resulting after cutting the vertices, producing pentagonal faces in their place (see Synopsis 9). As is well known, the C_{60} fullerene can be presented as a collection of twelve formally independent pentagons. The left side of the synopsis 9 shows the formation of hexagons with alternating l_1 and l_2 bond lengths, where l_1 denotes the edge common with the pentagon. If denote by L the length of the edge of the parent icosahedron, one observes that we have $L=2l_1+l_2$, considering that the triangles from the faces of the removed pyramidal tops are equilateral. From here, the following relationships are resulting:

$$\frac{R_l}{L} = \frac{1}{2} \sqrt{1 + \gamma^2} \quad (11.a)$$

$$\frac{H}{L} = \frac{1}{2} \gamma \quad (11.b)$$

Here, γ is the Golden Number, $\gamma = (1 + \sqrt{5}) / 2$.



Synopsis 9. Left side: the obtaining of C_{60} polyhedron as truncation of the icosahedron vertices. The pentagonal faces have edges with l_1 length, while the hexagonal ones are alternating the l_1 and l_2 lengths. Middle panel: section comprising one edge of the icosahedron, with L length, and the isosceles triangle formed with the center of symmetry, having the R_l values for the other two edges and the H height. The nodes of the C_{60} polyhedron are marked by dark circles, the radius R of the vertices being the hypotenuse of the triangle with H and $l_2/2$ edge lengths. Right side: The independent atom atom species with respect of in the T_h cubic group. The atom types correspond to the a , b and c labels in Table 1. The + and – subscripts for the (a) type represent the change of sign x coordinate.

The analytic expression of Cartesian coordinates of the fullerene is shown conveniently descending from the icosahedral I_h point group to the T_h cubic subgroup. Obviously, with respect of icosahedron symmetry, there is an unique species of cluster atoms, but is convenient to take the cubic format, where are three species, because their symmetry multiplication to the whole C_{60} can be expressed as permutation of signs and coordinates. The table 4 shows the three atom types labelled a , b and c and their Cartesian coordinates as function of the above defined radial and tangential parameters. In the right side of synopsis 9 is illustrated the symmetry retrieval of a fragment resembling a naphthalene skeleton starting from the Table 4 expressions. Note that the C_{60} can be presented as the six time repeated C_{10} naphthalene-like moiety, taking cyclic permutations and inversions of the x , y and z coordinates.

The radius R of the nodes of the fullerene polyhedron can be determined as the hypotenuse of the triangle having the edges with H and $l_2/2$ lengths:

$$R = \sqrt{H^2 + \frac{1}{4}l_2^2} = \frac{1}{2}\sqrt{\gamma^2 L^2 + l_2^2} = \frac{1}{2}\sqrt{4\gamma^2 l_1^2 + (1 + \gamma^2)l_2^2 + 4\gamma^2 l_1 l_2} \quad (12)$$

Let us define the tangential parameter τ ,

$$\tau = \frac{l_1}{l_2} - 1, \quad (13)$$

measuring the deviation of the bond length ratio from the situation of their equality. The reverse relation, between radial and tangential, R and τ , to the carbon-carbon bond lengths is:

$$l_1 = 2(1 + \tau)f \cdot R , \quad (14.a)$$

$$l_2 = 2f \cdot R , \quad (14.b)$$

implying the factor f defined as follows:

$$f = \frac{R}{\sqrt{1 + \gamma^2(3 + 2\tau)^2}} . \quad (15)$$

The analytic expression of Cartesian coordinates of the fullerene are shown conveniently descending from the icosahedral I_h point group to the T_h cubic subgroup, as shown in Table 4.

Table 4. Analytic expression of independent Cartesian coordinates with respect of atom species conveniently taken in the T_h cubic group. The atom types correspond to the a , b and c labels from Synopsis 9. The factor f is $f = R / \sqrt{1 + \gamma^2(3 + 2\tau)^2}$

Type	x	y	z
a	f	0	$(3 + 2\tau) \cdot f$
b	$(2 + \tau) \cdot f$	$(1 + \tau) \cdot f \cdot \gamma$	$(1 + 2\gamma + \tau + \gamma\tau) \cdot f$
c	$(1 + \tau) \cdot f$	$(2 + \tau) \cdot f \cdot \gamma$	$(2 + \gamma + \tau + \gamma\tau) \cdot f$

The analytic handling of Cartesian coordinates enables the expression of the two totally vibration coordinates encountered for the C_{60} icosahedral system. The definition of the modes consists in taking the derivatives of above discussed Cartesian coordinates with respect of the driving R and τ parameters.:

$$q_R^i = \frac{d}{dR} \{x_i, y_i, z_i\}, \quad (16.a)$$

$$q_\tau^i = \frac{d}{d\tau} \{x_i, y_i, z_i\} . \quad (16.b)$$

The resulting movements are represented in Synopsis 10.

The vibration energies of the A_g modes are obtained as solution of the determinant:

$$\begin{vmatrix} V_{RR} - M_{RR} \cdot \lambda & V_{R\tau} \\ V_{R\tau} & V_{\tau\tau} - M_{\tau\tau} \cdot \lambda \end{vmatrix} = 0, \quad (17),$$

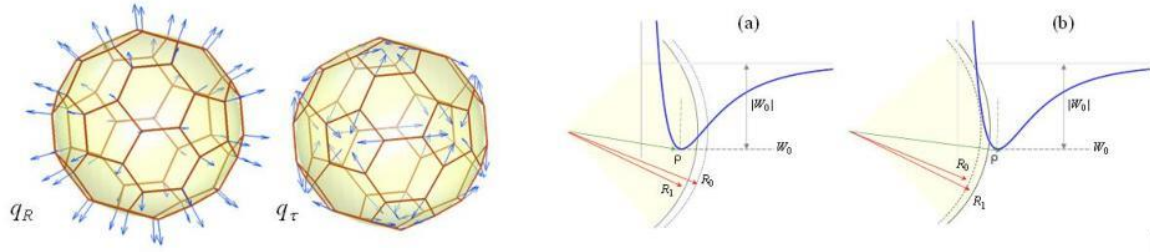
where

$$V_{RR} = \frac{\partial^2 E}{\partial R^2}, \quad V_{R\tau} = \frac{\partial^2 E}{\partial R \partial \tau}, \quad V_{\tau\tau} = \frac{\partial^2 E}{\partial \tau^2}, \quad (19)$$

are the force constant matrix elements, while the M masses of the modes are:

$$M_{RR} = 60m_C, \quad M_{R\tau} = 0, \quad M_{\tau\tau} = \frac{1920(5 + 2\sqrt{5} + 2(7 + 3\sqrt{5})\tau + 2(7 + 3\sqrt{5})\tau^2)}{(5 + \sqrt{5} + 4(3 + \sqrt{5})\tau + 4(3 + \sqrt{5})\tau^2)^3} m_C R^2, \quad (20)$$

with m_C the carbon atom mass.



Synopsis 10. The total symmetric vibration coordinates, radial, q_R and tangential q_τ . Scheme of the radial geometry and vibrational shifts in endohedral fullerenes.

In order to extract the parameters of van der Waals interaction between the noble gas and the fullerene inner walls, we will equate the small shifts in the equilibrium radius and in the force constant of the breathing radial vibration, when compare the filled fullerene with the empty cage.

We express the endohedral fullerene as the harmonic potential of the radial vibration (breathing mode) of the fullerene, plus the van der Waals interaction between central and cage atoms, taken in a Lennard-Jones format:

$$E(R) = \frac{1}{2} V_{RR}^0 (R - R_o)^2 + W_0 \left(2 \frac{\rho^6}{R^6} - \frac{\rho^{12}}{R^{12}} \right), \quad (21)$$

where R_0 is the equilibrium radius of the fullerene, ρ is the expected position for the minimum of the Lennard-Jones potential and W_0 the van der Waals energy stabilization. Filled with the noble gas atom, the fullerene cage acquires a new equilibrium distance, equated as the quenching of the first derivative with respect of the radial parameter

$$\left(\frac{d}{dR} E(R) \right)_{R=R_1} = V_{RR}^0 (R_1 - R_o) - 12W_0 \left(\frac{\rho^6}{R_1^7} - \frac{\rho^{12}}{R_1^{13}} \right) = 0 \quad (22)$$

The second derivative will give an amount to be connected with the vibration shift, as the new force constant:

$$\left(\frac{d^2}{dR^2} E(R)\right)_{R=R_1} = V_{RR}^1 = V_{RR}^0 + 12W_0 \left(7\frac{\rho^6}{R_1^8} - 13\frac{\rho^{12}}{R_1^{14}}\right) \quad (23)$$

The above equations are carrying the information necessary to obtain the two Lennard-Jones parameters.

The ρ minimum of the van der Waals curve is in the relative proximity of the R_0 radius of the fullerene. There are two possibilities, depicted in the (a) and (b) panels. When the R_0 fullerene radius falls in the attractive part of the potential ($\rho < R_0$) there is the trend towards the contracted radius of the endohedral cluster, $R_1 < R_0$. By contrary, the placement in the repulsive part ($\rho > R_0$) will determine the expansion of the cluster, to release the tension (see Synopsis 10).

Table 5. Parameters of Lennard-Jones curve for the noble gas-fullerene interaction (W_0 in kcal/mol and ρ in Å), the shift of radial total symmetric vibration shift ($dv_R(A_g)$ in cm^{-1}) and fullerene radius shift (dR , in Å, magnified by a factor of 1000), compared with vibration and radius of empty C_{60} , computed with range uncorrected methods and 6-311G* basis set. The methods in first column have the same acronym like in Gaussian input command line.

Method	System	W_0 kcal/mol	ρ (Å)	$dv_R(A_g)$ (cm^{-1})	$dR \cdot 10^3$ (Å)
HF	Ar@C ₆₀	45.8	3.100	0.21	2.28
HF	Kr@C ₆₀	71.8	3.090	0.44	3.57
SVWN	Ar@C ₆₀	20.6	3.566	-2.48	-0.41
SVWN	Kr@C ₆₀	29.1	3.506	-2.54	0.15
BP86 ^a	Ar@C ₆₀	30.9	3.477	-1.79	0.85
BP86	Kr@C ₆₀	54.7	3.446	-2.58	1.92
BLYP	Ar@C ₆₀	16.6	3.400	-0.47	0.76
BLYP	Kr@C ₆₀	55.5	3.422	-2.01	2.36
B3LYP ^b	Ar@C ₆₀	38.3	3.376	-1.22	1.63
B3LYP	Kr@C ₆₀	57.2	3.398	-2.12	2.25

Table 6. Parameters of Lennard-Jones curve for the noble gas-fullerene interaction (W_0 in kcal/mol and ρ in Å), the shift of radial total symmetric vibration shift ($dv_R(A_g)$ in cm^{-1}) and fullerene radius shift (dR , in Å, magnified by a factor of 1000), compared with vibration and radius of empty C_{60} , computed with range uncorrected methods and 6-311G* basis set. The methods in first column have the same acronym like in Gaussian input command line.

Method	System	W_0 kcal/mol	ρ (Å)	$dv_R(A_g)$ (cm^{-1})	$dR \cdot 10^3$ (Å)
LC-SVWN	Ar@C ₆₀	36.0	3.278	-0.76	1.64
LC-SVWN	Kr@C ₆₀	53.4	3.229	-0.60	2.61
LC-BP86	Ar@C ₆₀	4.9	3.446	-0.38	0.08
LC-BP86	Kr@C ₆₀	-	-	0.65	0.82
LC-BLYP	Ar@C ₆₀	18.0	3.164	-0.09	0.92
LC-BLYP	Kr@C ₆₀	36.2	3.093	0.15	1.87
LC-WPBE	Ar@C ₆₀	38.1	3.377	-1.52	1.38
LC-WPBE	Kr@C ₆₀	41.2	3.126	0.11	2.16
CAM-B3LYP	Ar@C ₆₀	32.8	3.325	-0.77	1.50
CAM-B3LYP	Kr@C ₆₀	52.9	3.324	-1.19	2.43
HSEH1PBE	Ar@C ₆₀	39.9	3.454	-2.40	0.95
HSEH1PBE	Kr@C ₆₀	45.0	3.380	-1.61	1.76
M11	Ar@C ₆₀	63.7	3.546	-6.44	-0.32
M11	Kr@C ₆₀	12.8	3.330	-0.31	0.59

Table 7. Parameters of Lennard-Jones curve for the noble gas-fullerene interaction (W_0 in kcal/mol and ρ in Å), the shift of radial total symmetric vibration shift ($dv_R(A_g)$ in cm^{-1}) and fullerene radius shift (dR , in Å, magnified by a factor of 1000), compared with vibration and radius of empty C_{60} , computed with functionals corrected with dispersion increments and 6-311G* basis set. The methods in first column have the same acronym like in Gaussian input command line.

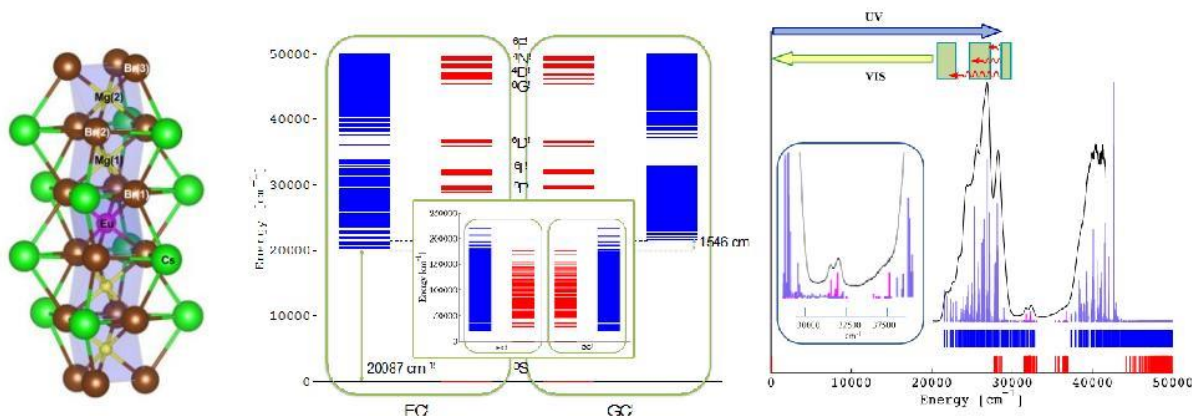
Method	System	W_0 kcal/mol	ρ (Å)	$dv_R(A_g)$ (cm^{-1})	$dR \cdot 10^3$ (Å)
B3LYP D2	Ar@C ₆₀	7.0	3.546	-0.71	-0.01
B3LYP D2	Kr@C ₆₀	19.6	3.358	-0.57	0.88
B3LYP D3	Ar@C ₆₀	-	-	0.35	0.46
B3LYP D3	Kr@C ₆₀	47.2	2.831	0.71	1.99
B3LYP GD3BJ	Ar@C ₆₀	-	-	0.55	0.60
B3LYP GD3BJ	Kr@C ₆₀	44.4	3.226	-0.14	2.27
B97D	Ar@C ₆₀	-11.9	3.470	0.71	-0.33
B97D	Kr@C ₆₀	-69.0	3.567	7.04	0.30
B97D3	Ar@C ₆₀	-14.2	3.663	2.14	0.65
B97D3	Kr@C ₆₀	-34.9	3.687	5.82	2.08
WB97XD	Ar@C ₆₀	57.4	3.454	-3.48	1.36
WB97XD	Kr@C ₆₀	-141.6	3.587	16.95	3.25
APFD	Ar@C ₆₀	5.5	3.734	-1.38	-0.68
APFD	Kr@C ₆₀	6.5	3.533	-0.64	-0.01

Concluding the results of this objective, we note again that the proposed particular systems, the noble gas endohedral fullerenes, Ng@C₆₀ (Ng=Ar, Kr), are putting a severe test on the account of van der Waals interaction and rise several methodological concerns. An issue is the impossibility to draw a complete profile of the potential by fitting Lennard-Jones parameters of the Ng-C contacts when tuning the radius of the fullerene cage, since the change of energy at dissociating the C-C bonds overrides the non-covalent effects. We proposed an original model circumventing this problem, by equating the shift of vibration frequencies of the breathing mode in the C₆₀ vs. Ng@C₆₀ comparison, aside with the slight alteration of fullerene radius. A

transparent analytical model enables in this way the Lennard-Jones parameters for the Ng@C₆₀ systems, as function of the computation method. The advent of this method consists in the fact that the range of desired van der Waals association energies is the same with the input quantities of the model (vibration frequencies), namely in the scale of 10⁻³ Hartree. This avoids the obtaining of small intermolecular interactions as difference of total molecular energies, six order of magnitude larger. Another positive issue is the circumventing of the need for counterpoise correction of the basis set superposition errors. The calculations compared the 6-311G* and 6-311+G* basis sets and various functionals, grouped in three categories: genuine uncorrected forms (pure and hybrid), long range corrected functionals and species with empirical dispersion ingredients. As expected, the genuine functionals are undergoing failures. The long range corrections to pure functionals record several successes, particularly with the richer basis set. Methods rated with more advanced range corrections are showing however systematic failures. Several methods based on Grimme-type dispersion terms are successfully accounting the trends. However, the vast majority of the tested functionals, even those designed for the use in intermolecular interaction problems, are failing to account expected trends in the vibrational shifts at encapsulation and to render the Lennard-Jones parameters, after the designed handling of the computation data. The DFT appears still problematic in the account of subtle supra-molecular effects, the empirical corrections seeming a practical compromise. At the same time, long range correction procedures, particularly those designed for pure functionals, following a clear concept, are also promising, with better results at richer basis sets.

Interactions in supra-molecular host-guest tubular systems. Elaborating original models for the estimation of the non-covalent interactions..

Without detailing this subject, we present just a synoptic view on the treatment of the Ligand Field type non-covalent interactions of the Eu(II) ion, encapsulated in a tubular cluster of bromide and magnesium ions. The treatment is similar to those exposed in the previous sections for fullerenes incorporating lanthanide ions and is relevant for the phosphor properties (the study considering the context of year 2015, declared as International Year of Light and Illumination Technologies).



Synopsis 11. Structure and spectral properties of the Eu(II) ion encapsulated in a tubular cluster, $\{Mg_{12}Br_{18}\}$, a system special optical properties.

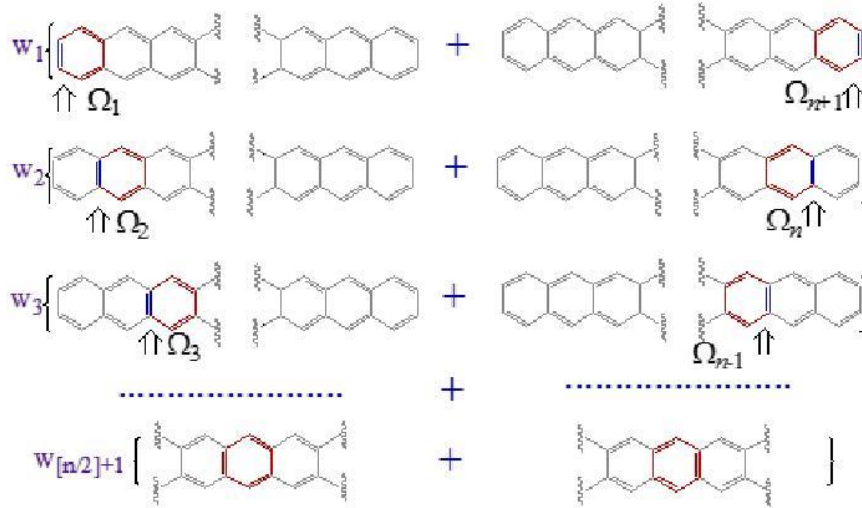
Spin coupling, special magnetic and electric properties and conduction in carbon systems with extended conjugation.

This subject represents the preliminary approach of next year objectives. The Poly-Aromatic Hydrocarbons (PAH)³⁹ show, in their variety of molecular topologies, a set of potentially useful properties for concepts of nanostructured devices, opto-electronics or magnetics⁴⁰. For instance, polymeric semiconducting PAH systems are largely employed in thin displays. Also, the PAH molecules are used as theoretical and experimental case studies in the concern of spin and charge transfer through nanometric sized molecular entities embedded between metallic electrodes⁴¹ or in the design of devices for tentative applications in spintronics or molecular electronics.

Starting from the idea that the electronic delocalization is the engine for the conducting properties, we will speculate a molecular approach of this effect, using spin coupling modelling and polyacenes as appropriate cases. One can make a parallel with the situation of molecular magnetism,⁴² which has grown translating in the language of structural chemistry concepts basically known in terms of solid state theories (Anderson 1959). The actual models of conduction are yet tributary to concepts merely familiar to physicists, such as the ballistic transport phenomenology. Now we attempt to turn the explanation in a manner transparent to the chemical intuition, proposing the resonance structures from Valence Bond formalism as designated drivers of spin and charge, the linear polyacenes being particularly suited for this point.

The polyacenes are polycyclic conjugated hydrocarbons with $C_{4n+2}H_{2n+4}$ general formula, the simplest pattern being the linear condensation of benzenoid rings. In idealized mode, the linear polyacenes are planar, spanning the D_{2h} point group. The series starts with, naphthalene ($n=2$) and

anthracene ($n=3$), ending with heptacene ($n=7$), the highest known congener.⁴³ Although small as extension, the class shows various optical and electric properties⁴⁴ with potential interest for material sciences and nanotechnologies. Thus, the polyacenes are able to trigger laser effects⁴⁵ and their films are semiconductors.⁴⁶ The interesting manifestations are accentuated with the increased dimension, being correlated with the progressive reduction of the gap between occupied and virtual orbitals, and also parallel with the trend toward the crossing of singlet and triplet states.⁴⁷ The lower gap from groundstate to triplet determines the reactivity of the high analogues and, presumably, the ending of the series when a quasi-degenerate situation is reached.



Synopsis 12. The scheme of resonance structures of polyacenes, formulated as a “vertical” double bond traveling from one side of the molecule to the other. The structures are arranged in equivalent couples, related with the mirroring through the middle of the molecule.

At a more sophisticated level, though yet phenomenological, based on the Heisenberg Spin Hamiltonian, each resonance structure corresponds to a wavefunction obtained by taking spin-paired products with one spin on each C atom:

$$\Omega_i = \frac{1}{\sqrt{2^{n+1}}} \left\{ \prod_{k=1}^{j-1} (\alpha_{2k} \beta_{2k} - \beta_{2k-1} \alpha_{2k}) \prod_{k=1}^{j-1} (\alpha_{2n+2k} \beta_{2n+2k+1} - \beta_{2n+2k} \alpha_{2n+2k}) \right\} \cdot \{ (\alpha_{2j+1} \beta_{2n+2j+2} - \beta_{2j+1} \alpha_{2n+2j+2}) \} \cdot \left\{ \prod_{k=j+1}^n (\alpha_{2k} \beta_{2k+1} - \beta_{2k} \alpha_{2k+1}) \prod_{k=j+1}^n (\alpha_{2n+2k+1} \beta_{2n+2k+2} - \beta_{2n+2k+1} \alpha_{2n+2k+2}) \right\} \quad (23)$$

Such states can be used as basis for a limited configuration interaction with the Heisenberg Spin Hamiltonian:

$$\hat{H} = \sum_{j < i} \left(-2 \hat{S}_i \cdot \hat{S}_j - 1/2 \right) J_{ij} \quad (24)$$

The clue for considering polyacenes as playground for the conduction models is sketched in the Synopsis 12. Namely, one may observe that taking Kekulé –type resonance structures, drawing for convenience the paired couples as double bonds (instead of the previously used arrows), only one pairing has a “vertical” placement. The “vertical” labelling comes putting the molecule with the long axis horizontally. A polyacene with n benzene rings, having a C_{4n+2} carbon content, can be regarded as made of two C_{2n+1} polyene chains, going in zig-zag along the horizontal axis, connected by $n+1$ vertical carbon-carbon bonds. When draw the resonance, from the total of $2n+1$ double bonds, n are placed in one polyene moiety, other n being symmetrically in the other fragment, while one double bond goes vertically. One may place this “vertical” couple in any of the $n+1$ vertical carbon-carbon linkages. Then, a n -polyacene has $n+1$ Kekulé resonances. Running the “vertical” double bond for one side of the molecule to the other can be formally regarded as the traveling of an electron couple along the molecular wire represented by the skeleton of the linear molecule.

The resonances, labelled Ω_i , can be enumerated according to the i -th position of the vertical double bond determining entirely their pattern. Without detailing the derivation, we can present general formulas for the overlap and matrix elements in the basis of Kekulé structures of linear polyacenes:

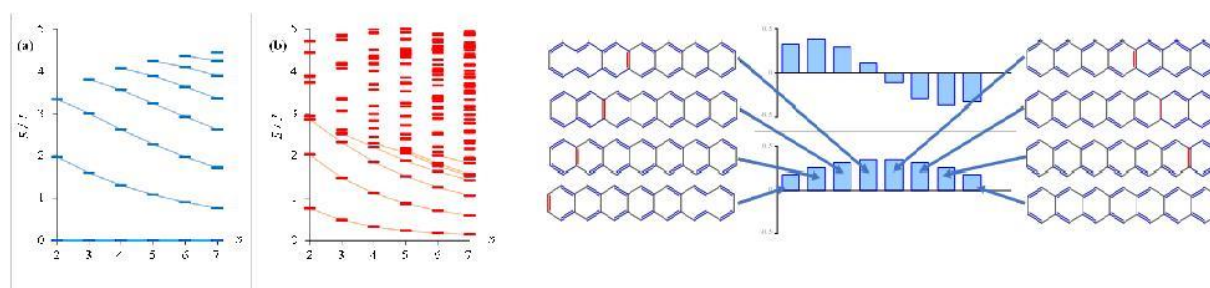
$$H_{i,j} = \langle \Omega_i | \hat{H} | \Omega_j \rangle = \left(\frac{1}{4} \right)^{|i-j|} \frac{1}{2} (n+2+9|i-j|) \cdot J \quad (25.a)$$

$$S_{i,j} = \langle \Omega_i | \Omega_j \rangle = \left(\frac{1}{4} \right)^{|i-j|} \quad (25.b)$$

With these equations we can easily investigate the full spectrum of VB-alike states in large polyacenes, under the simple assumption of Kekulé basis sufficiency. Besides, we will consider also the triplet states. For this goal, we cannot derive analytic expressions, remaining to be evaluated numerically. We will also introduce an assumption on the basis of the triplet resonances. Namely, we propose the successive decoupling into pairs of α electrons of the couples from a singlet Kekulé reference. Thus, from a Kekulé structure having N couples one may draw N triplets, running the unpaired sites over the former bonding linkages. Thus, for a n -polyacene, having $2n+1$ electron pairs and $n+1$ singlet resonances, we get a triplet basis with $(n+1)(2n+1)$ dimension. With this model settled, we drawn the series of spectra from the Synopsis 13.

The left panel shows the singlet states, observing the progressive decrease of the gap between ground and first excited state. This parallels the trend expected from molecular orbital diagrams, although the spin Hamiltonian has not an explicit connection with these methods. A very interesting aspect is noticed in the middle panel, showing the triplet states relative to the singlet

ground level. One finds a rapid reduction of the singlet-triplet gap, which becomes very small nearby the $n=7$ congener. This can be nicely correlated with the above mentioned fact, that heptacene is the last member of the series available experimental. The very low triplet levels after this critical point are making the molecule prone to the reactive degradation. Thinking on the oxidation processes, it is well known that these are kinetically hindered for organic compounds (while thermodynamically allowed) by the fact that singlet-triplet processes are spin forbidden. Indeed, the organic systems are usually singlets (closed shell or complete spin paired structures), while the oxygen molecule has a triplet groundstate. When the molecules show low triplet states, these can get in interaction, making the interaction with oxygen strong, opening the gate for the further degradation steps.



Synopsis 13. Left side: The spectra of spin coupled states for the series of linear polyacenes with n running from $n=2$ to 7. The singlet states are in blue, while the triplets in red. Right side: The hysterograms of the coefficients from the eigenvectors of the first two spin coupled states (groundstate and the first excited level) for the heptacene example ($n=7$). The resonance structures forming the basis are represented on the margins, pointing the links to their corresponding coefficient in the groundstate.

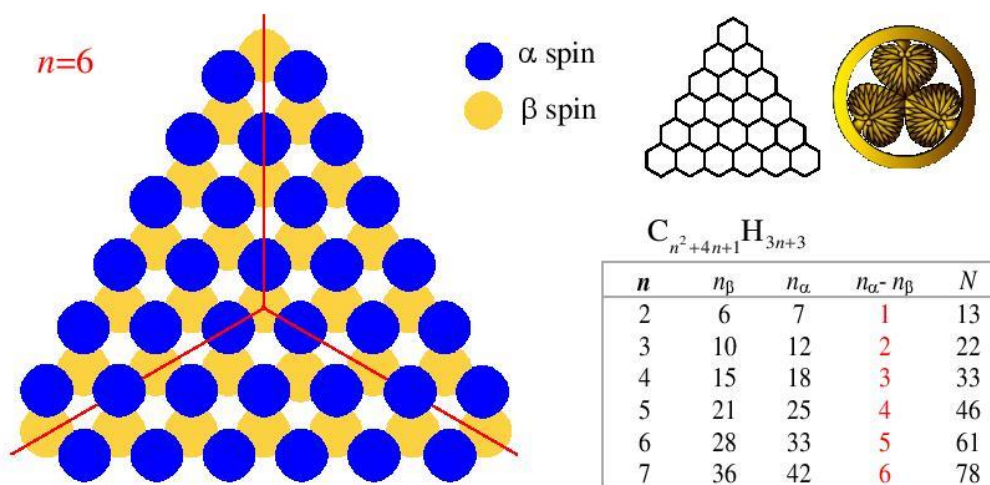
One observes that the coefficients are growing from margins to the middle. The resonances having the double bonds nearby the middle of the molecule are getting higher participation. This can be understood well in heuristic manner. The resonance takes place between symmetry equivalent objects, namely structures related by mirror or rotation elements. However, the energy gains are not equal for all such couples. One may intuitively guess that the structures having distant “vertical” linkages, such as the Ω_1 - Ω_8 couple, are less effective for the resonant stabilization. In turn, in the given example, the Ω_4 - Ω_5 couple gives the most definite aromatic stabilization. Then, since the most stabilizing contributions are coming from resonance structures running Kekulé conjugation on the rings from the middle of the molecule, one may understand that these gain main weights in the groundstate. In other words, the aromaticity of linear polyacenes can be considered as concentrated at the middle of the molecules.

The first excited state has the same symmetry like a vector directed on the long molecular axis. Given the opposite parity of ground and excited state (even vs. odd), their coupling can be

achieved by perturbations with polar nature, such as a properly oriented electric field. Their mutual mixing is stronger when the ground-excited gap is reduced. One may rationalize in this way the conduction properties of large polyacenes. These correlations are supporting the outlined idea, of considering the conduction along polyacene as the travel of the representative “vertical” bond from one margin to the other, when driven by electric field polar perturbation.

Special magnetic properties in carbon-based systems with extended conjugation. Triangular graphenes with spin.

We developed our investigation in the continuation of earlier preoccupation of triangular shaped graphene-type molecules where unpaired spins can appear in the groundstate, by topological reasons.⁴⁸ It was early recognized that in hydrocarbons with appropriate topology, unpaired electrons can be lodged in sets of quasi-degenerate orbitals (or even degenerate in limits of Hückel schemes).⁴⁹ This opens the challenging idea of the organic molecular magnetism and carbon-based magnetic materials.⁵⁰ Shaping graphene flakes in appropriate patterns, one may meet the situation of topologically unpaired spins⁵¹. We will consider the idealized version of this class, taking equilateral triangles made from benzenoid cells. A short introduction of the topological spin in triangulenes is suggested in the synopsis from the Synopsis 14.



Synopsis 14. The synopsis of topologically determined spin in equilateral triangulenes with $C_{n^2+4n+1}H_{3n+3}$ formula, where n is the number of hexagon units at one edge.

The example from Synopsis 14 corresponds to $n=6$, the molecular skeleton being shown as inset in the upper-right quarter. The left side suggests the excess of α alpha electrons resulting from the reasons of spin polarization topology. The simplest idea about the chemical bonding as spin pairing is arranging the alternation of α and β electrons on neighbour sites. Thus, counting the blue balls standing for α spins and the yellow ones as β electrons, one obtains the respective 33 vs. 28 result, having then a net spin $S=5/2$ from the excess of five spin-up particles. The counts for the $n=2-7$ series are exemplified in the table from right-down corner of the discussed synopsis. The combinatoric analysis of the general cases yields the following counts of the up and down total electronic populations:

$$n_{\alpha} = \frac{1}{2}n \cdot (n+5) \quad (26.a)$$

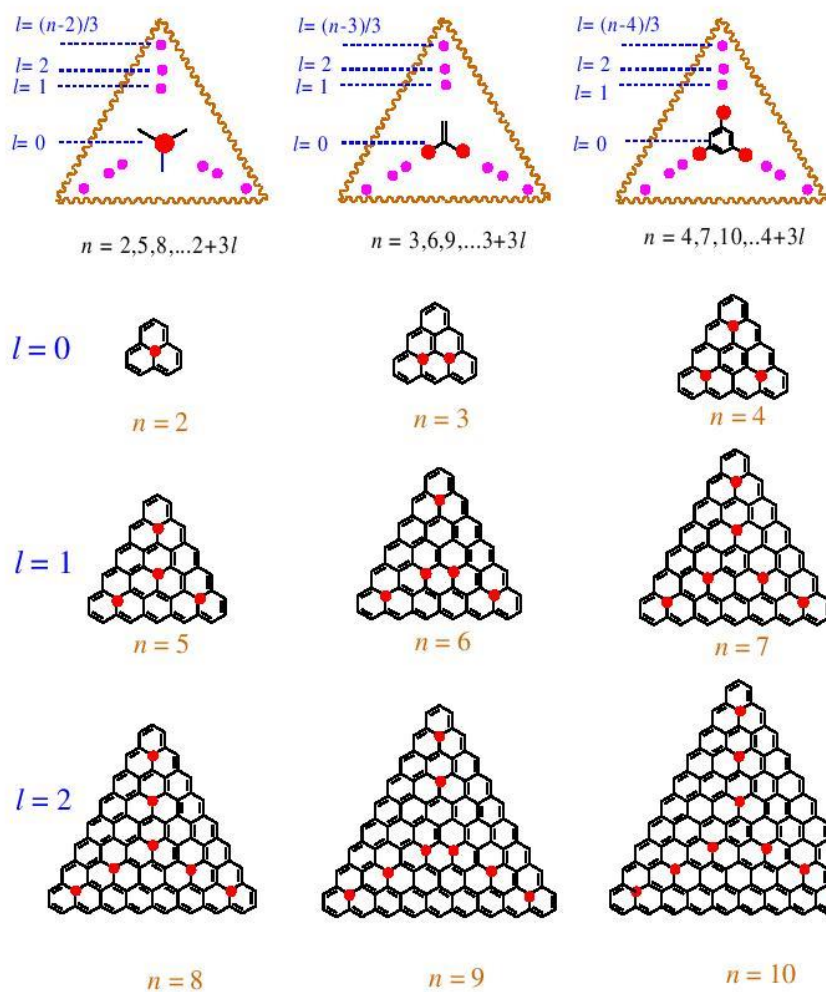
$$n_{\beta} = \frac{1}{2}(n+1) \cdot (n+2) \quad (26.b)$$

the corresponding spin multiplicity of a regular n -triangulene being:

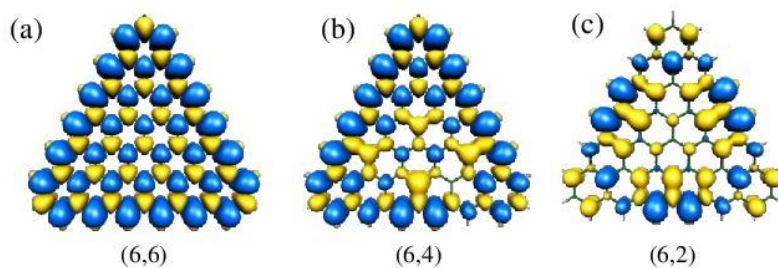
$$2S+1 = 2(n_{\alpha} - n_{\beta})/2 + 1 = n \quad (27)$$

We observe that there are three classes of triangular polyenes, according to the topology of the resonance structure with the highest imaginable symmetry. The corresponding “periodic” table is shown in the Synopsis 15. Thus, we identify three types of structures. The first one, starts with the simplest element, at $n=2$, being characterized by the fact that the symmetry center is occupied by carbon atom. The following congeners obeying this typology are at n equal to 5 and 8, drawing the $n=2+3l$ regularity, with the integer indices $l=0,1,2,\dots$ etc. If attempt to draw the resonance structure with the highest formal symmetry, the α electrons are placed as follows: one at the central carbon atom and the remaining ones on three equivalent lines going from center to vertices.

The following class starts with $n=3$, spanning the $n=3+3l$ cases. These molecules have also a carbon atom at the symmetry center, but if attempt to draw a symmetric resonance structure, one observes that this cannot obey the full D_{3h} symmetry, getting at most a C_{2v} pattern. The central region of this type of resonance can be described as a $C=C(\cdot)_2$ core having the broken symmetry of a double bond aside a biradical moiety. The last class runs over the $n=4,7, \dots 4+3l$ total counts of edge rings. It is characterized by having a hexagonal ring at the molecular center (the symmetry point being placed in its central void). The high symmetry resonance structure obeys the D_{3h} point group, the dots symbolizing the unpaired spins being placed on the lines radiating from the 1, 3 and 5 peripheral positions of the central hexagonal ring. To the best of our knowledge, this classification of triangulenes was not presented before.



Synopsis 15. The three topological classes of triangulenes, starting with the $n=2, 3$ and 4 counts (hexagons on the edge). The growth inside each class is controlled by the l index corresponding to the progressive addition of perimeter shells.



Synopsis 16. The spin density maps from unrestricted DFT calculations on different multiplicities of the $n=6$ triangulene. The α spin density is shown in blue, while the β one is drawn in yellow. The indices in parentheses denote the $(n, \text{multiplicity})$ values.

The spin polarization on large triangular graphenes is illustrated in the Synopsis 16 for the $n=6$ case. One may see that the alternation of α and β spin densities from the Fig.16(a) panel matches well the qualitative scheme drawn by intuition in the Synopsis 14. The groundstate of the 6-triangulene is a spin sextet. The (b) and (c) panels are illustrating other possible spin multiplicities, with lower value, namely quartet and doublet. The quartet state is breaking the trigonal symmetry of the molecule, the spin map getting a C_{2v} appearance, with the axis passing through the upper vertex and the central carbon atom. The spin doublet state gets again the trigonal symmetry, showing the segregation of spin-up densities on the edges, while the spin-down counterpart is polarized in the central area. In fact, also in the case of high spin state, the effective accumulation of the spin also occurs on edges. The spin map density is not directly illustrating this fact, but the analysis drawn in the Synopsis 17 offers details.

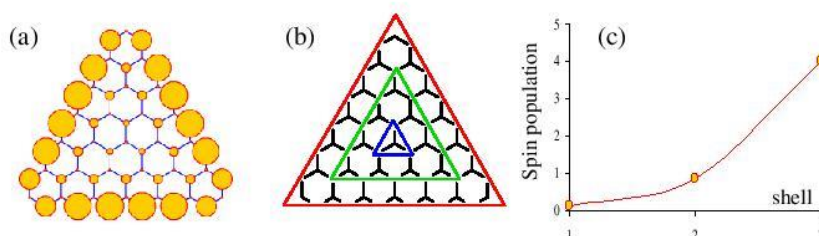


Fig. 17. Population analysis of the 6-triangulene, based on restricted open shell DFT calculation. The panel (a) shows the Mulliken spin populations on atoms, by circles drawn at relative scale. The panel (b) defines the partition of the molecule in three shells. The panel (c) draws the total spin population cumulated on the defined shells, numbered 1, 2 and 3, from inside to the periphery, respectively.

The large graphenes are yet a matter of imagination, brought to a certain concreteness with the help of first-principles simulations. However, there are e-beam lithography techniques that can tailor 2D nanoscale aromatic fragments with triangular patterns, starting from graphite.⁵² At the same time, important steps were already made in the synthesis and experimental characterization of the first members of the series. Thus, the nucleus of the $n=2$ structure, called phenalenyl, is present (in substituted form) in several derivatives well characterized, with X-ray structural data available,⁵³ and confirmed to have magnetic properties by electron spin resonance (ESR) and magnetic susceptibility measurements.⁵⁴ Moreover, derivatives of the $n=3$ congener, named triangulene (from which the name of the whole series was generalized), were synthesized and proven to carry spin.^{55,56} The variety of the species with this root is not very large, but is yet a firm promise of the carbon based spin chemistry.

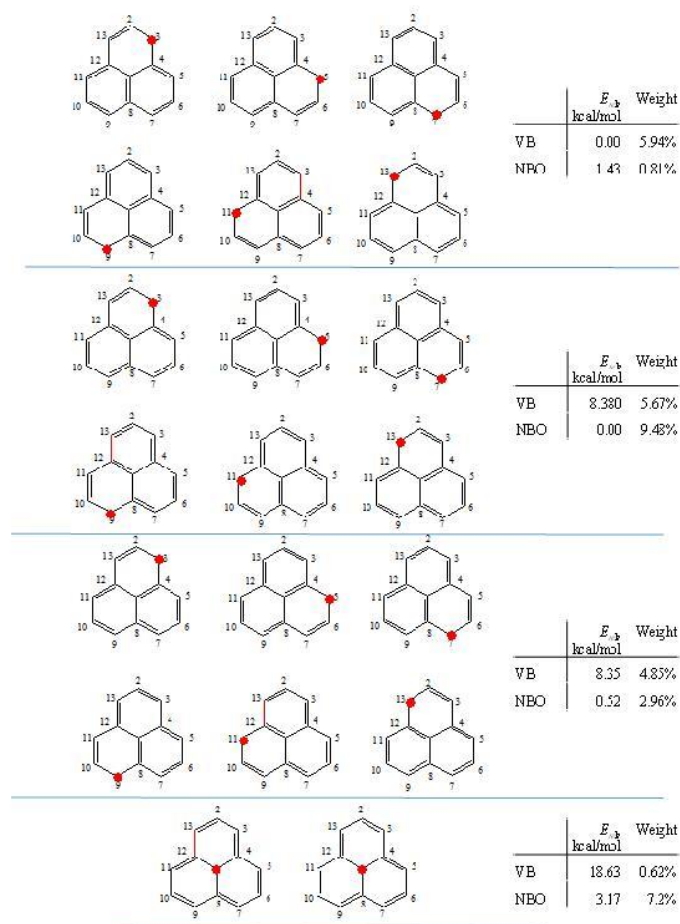
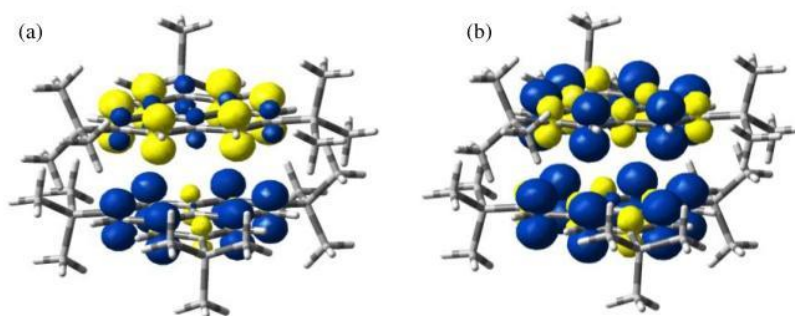


Fig.18 Resonance structures of the $n=2$ triangulene (the phenalenyl radical), grouped on classes of equivalence (separated by horizontal lines). For each class the results of Valence Bond (VB) calculations and Natural Bond Orbitals (NBO) post computation analyses of DFT results are shown comparatively.

Pedantically, the aromatic molecules with topological spin can be characterized as non-Kekulé systems, because the skeleton cannot be drawn with defined bonds. However, in a more permissive terminology, we will consider as Kekulé-type the resonances that imply spin coupling along the connected sites only, namely excluding the Dewar-like lines between distant centres. Defined in this way, the Kekulé basis of the phenalenyl has 20 resonance structures, shown the Synopsis 18. The rather large number of resonances suggests already, as qualitative guess, the significant aromaticity of this system. There are 13 π electrons, comparable then with anthracene (with 14 electrons), for which only four Kekulé structures are available. A non-trivial achievement is the VB calculation done in this set of resonance structures, using the VB2000 code.⁵⁷ Due to the mutual placement of the spin coupled linkages (figured as double bonds),

aside the position of the radical, the resonance structures are falling in four different classes, grouped correspondingly in the Synopsis 18.

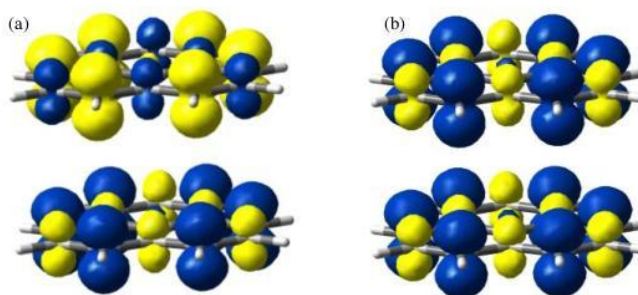
The parallel analysis in the frame of NBO (Natural Bond Orbitals)⁵⁸ and NRT (Natural Resonance Theory)⁵⁹ is comparatively annotated aside the VB briefing in the sections of the Synopsis 18. The results are not well correlated with the VB results. E.g., the two symmetric resonance structures with low VB weights are getting a rather high percentage, 7.2% in the NRT version. The confusion is also increased by the fact that in the case of the systems with spin, the code takes only the unrestricted orbitals. In this conjuncture, one obtains disjoint sets of NRT weights for the α and β subsystems. These two schemes are, indeed, not well correlated into an intuitively acceptable picture. For instance, the NRT decomposition of the β subsystem (which has a hole in the place of unpaired electron) yielded about 26% contribution for each of the two structures rated with low participation in the VB results. It is unfortunate that the NRT cannot function as replacement of the VB, since as mentioned, the VB approach becomes prohibitive for larger system.



Synopsis. 19. The spin density maps for experimental structure of dimeric 2,5,8-tri-tert-butyl-phenalenyl. Left side: the Broken Symmetry (BS) configuration having monomers with distinct α and β spin polarization (shown in blue and yellow, respectively). Right side, the High Spin (HS) configuration with overall α density. The monomers are mutually rotated by 180 degrees in their own mean planes.

At the end, we touch the problem of long range spin coupling, first taking the experimental structure of the supramolecular assemblies of 2,5,8-tri-tert-butyl-phenalenyl.⁶⁰ Thus, we apply Broken Symmetry DFT calculations²⁷ on a dimeric couple. The calculations are illustrated in the Synopsis 19. The distance between mean molecular planes is about 3.2 Å, the interaction being in the expected weak bonding range, where the method works. The approach consists in one unrestricted calculation for the system in high spin state (HS, namely parallel spins on the two monomers) and one calculation enforcing spin α at one fragment while spin β on the other, a pattern called Broken Symmetry (BS) configuration. The BS is not a real singlet state, but is a numeric experiment enabling information about the spin coupling strength. In more detail, a

dimer in singlet form should be described by a two-configurational wavefunction: $(\alpha_1\beta_2-\beta_1\alpha_2)$. The BS simulates only a single configuration, say the $\alpha_1\beta_2$ one. However, this is enough to extract useful data.



Synopsis 20. The spin density maps for hypothetical phenalenyl dimer when the molecules are imposed parallel (with equivalent atoms on the same verticals). Left side: the Broken Symmetry (BS) configuration. Right side, the High Spin (HS) configuration with overall α density. The distance between molecular planes is imposed 3.5 Å.

From the energy difference between the HS and BS results (divided by the corresponding difference of expectation values of the spin square operator, provided also by the output) one estimates the exchange coupling parameter J . This time, the J refers to the long-range interactions of the π -type orbitals from each subsystem, which in the intersystem mode are acting actually as distant and weak σ -like overlapping. We estimated a $J=-1960\text{ cm}^{-1}$ that describes the overall interaction of the stacked molecular planes. We provoked also the numeric experiment considering the parallel alignment of two monomers with eclipsed mutual orientation. The spin maps of the HS and BS configurations are drawn in the Synopsis 20. In this case, the carbon atoms from different units are aligned on the same vertical axis. Then, formally, one may divide the estimated inter-dimer exchange coupling by the number of atoms, to get the averaged parameter per carbon-carbon stacked pair. When inter-planar distance is tuned at 3.0Å, 3.5Å and 4.0Å, the inter-dimer exchange coupling, taken as overall value, varies as follows: -3440 cm^{-1} , -1262 cm^{-1} and -367 cm^{-1} , respectively. Divided per atom, one estimates the following dependence: -265 cm^{-1} , -97 cm^{-1} and -28 cm^{-1} . This numeric experiment provides valuable information for prospects of further modelling of stacking effects by spin-coupling formalisms.

Conclusions.

Using a large palette of methodological developments, assessed by applications related to the established milestones, we brought breakthrough contributions to the covered topics, with relevance for theoretical community, as well as interesting for a wider audience, by the opening toward the heuristic interpretation and the relationship with the experiment.

*
**

Results Summary

7 ISI papers were contracted and 14 ISI papers were realized.

In addition we produced

4 chapters book (Springer and IGI Global publishers)

1 book (Springer publishers),

All papers, book chapters and the book acknowledged the UEFISCDI support.

24 conferences (invited lectures, keynotes, oral presentations, posters, in national and international events) are published.

Papers:

14. Toader, A.M.; Buta, C.; Frecus, B.; Diudea, M.; Cimpoesu, F.

J. Chem. Theory Comput. **2016**, submitted.

13. Cimpoesu, F.; Buta, C.; Ferbinteanu, M.; Philpott, M.R.; Stroppa, A.; Putz, M.,

Curr. Org. Chem., **2016**, in press.

12. Frecus, B.; Buta, C.M.; Oprea, C.I.; Stroppa, A.; Putz, M.V.; Cimpoesu, F.,

Theor. Chem. Acc. **2016**, *135*(5), 133 (1-9).

11. Oprea, C.; Petcu, L.C.; Girtu, M.

E-Health and Bioengineering - EHB **2015**, DOI: 10.1109/EHB.2015.7391481.

10. Ramanantoanina, H.; Urland, W.; Herden, B.; Cimpoesu, F.; Daul, C.

Phys. Chem. Chem. Phys. **2015**, *17*(14), 9116-9125.

9. Ramanantoanina, H.; Sahnoun, M.; Barbiero, A.; Ferbinteanu, M.; Cimpoesu, F.

Phys. Chem. Chem. Phys. **2015**, *17*(28), 18547-18557.

8. Garcia-Fuente, A.; Cimpoesu, F.; Ramanantoanina, H.; Herden, B.; Daul, C.; Suta, M.;

Wickleder, C. ; Urland, W.

Chem. Phys. Lett. **2015**, *622*, 120-123.

7. Ramanantoanina, H.; Cimpoesu, F.; Gottel, C.; Sahnoun, M.; Herden, B.; Suta, M.; Wickleder,

C.; Urland, W.; Daul, C.

Inorg. Chem. **2015**, *54*(17), 8319-8326.

6. Cimpoesu, F.; Frecus, B.; Oprea, C.I.; Ramanantoanina, H.; Urland, W.; Daul, C.

Mol. Phys. **2015**, *113*(13-14), 1712-1727.

5. Ramanantoanina, H.; Urland, W.; García-Fuente, A.; Cimpoesu, F.; Daul, C.

Phys. Chem. Chem. Phys. **2014**, *16*(28), 14625-14634.

4. Frecus, B.; Oprea, C.I.; Panait, P.; Ferbinteanu, M.; Cimpoesu, F.; Gîrțu, M. A.

Theor. Chem. Acc. **2014**, *133*,1470.

3. Cimpoesu, F.; Frecus, B.; Oprea, C.I.; Panait, P., Gîrțu, M. A.

Comp. Mat. Sci. **2014**, *91*, 320-328.

2. Ramanantoanina, H.; Urland, W.; Cimpoesu, F.; Daul, C.

Phys. Chem. Chem. Phys. **2014**, *16*, 12282-12290.

1. Cimpoesu, F.; Dragoe, N.; Ramanantoanina, H.; Urland, W.; Daul, C.

Phys. Chem. Chem. Phys. **2014**, *16*, 11337-11348.

Book chapters:

4. Putz, M.V.; Cimpoesu, F.; Ferbinteanu, M.

New keys for Old Keywords. Hybridization and Aromaticity, Graphs and Topology

In *Structural Chemistry Principles, Methods, and Case Studies*, Springer, 2017, in press.

3. Ferbinteanu, M.; Buta, C.; Toader, A.M.; Cimpoesu, F.

The Spin Coupling in the Polyaromatic Hydrocarbons and Carbon-based Materials

In *Organic synthesis and carbon related materials- Dedicated to Nobel Laureate Prof. Akira Suzuki for his 85th birthday*, Springer, 2017, in press.

2. Ferbinteanu, M.; Ramanantoanina, H.; Barbiero, A.; Cimpoesu, F.

Bonding mechanisms and causal relationships with magnetic properties in extended

coordination systems: Case studies in the challenge of property design at nanoscale , in

Sustainable Nanosystems Development, Properties, And Applications, Eds.: Mihai V. Putz &

Marius C. Mirica, IGI publisher, 2017, in press. ISBN13: 9781522504924 DOI: 10.4018/978-1-5225-0492-4.

1. Ferbinteanu, M.; Cimpoesu, F.; Tanase, S.

Metal-Organic Frameworks with d-f Cyanide Bridges: Structural Diversity, Bonding Regime,

and Magnetism, in *Lanthanide Metalorganic Frameworks*, Ed. Peng Cheng,

Structure and Bonding 2015, 163, 185-229,

ISBN: 978-3-662-45772-6 (Print) 978-3-662-45773-3 (Online)

DOI: 10.1007/430_2014_156M, WOS:000348907100007.

Book:

Putz, M.V.; Cimpoesu, F.; Ferbinteanu, M. *Structural Chemistry Principles, Methods, and Case Studies*, Springer, **2017**, 800 pag., in press.

All papers, book chapters and book acknowledged the UEFISCDI support.

References

- ¹ H. Ramanantoanina, W. Urland, F. Cimpoesu and C. Daul, *Phys. Chem. Chem. Phys.*, **2014**, *16*, 12282-12290.
- ² F. Cimpoesu, N. Dragoie, H. Ramanantoanina, W. Urland, and C. Daul, *Phys. Chem. Chem. Phys.* **2014**, *16*, 11337.
- ³ (a) T. Kanbara, Y. Kubozono, Y. Takabayashi, S. Fujiki, S. Iida, Y. Haruyama, S. Kashino, S. Emura and T. Akasaka, *Phys. Rev. B* **2001**, *6411*, 113403. (b) T. Inoue, Y. Kubozono, S. Kashino, Y. Takabayashi, K. Fujitaka, M. Hida, M. Inoue, T. Kanbara, S. Emura and T. Uruga, *Chem. Phys. Lett.* **2000**, *316*, 381. (c) R. F. Sabirianov, W. N. Mei, J. Lu, Y. Gao, X. C. Zeng, R. D. Bolskar, P. Jeppson, N. Wu, A. N. Caruso and P. A. Dowben, *J. Phys.-Condes. Matter*, **2007**, *19*, 6.
- ⁴ (a) A. Á. Náfrádi, Á. Pásztor, L. Forró, L. F. Kiss, T. Fehér, É. Kováts, S. Pekker and A. Jánossy, *J. Phys. Chem. Lett.*, **2012**, *3*, 3291. (b) M. Treier, P. Ruffieux, R. Fasel, F. Nolting, S. Yang, L. Dunsch and T. Greber, *Phys. Rev. B*, **2009**, *80*, 081403. (c) J. Tang, I. J. Hewitt, N. T. Madhu, G. Chastanet, W. Wernsdorfer, C. E. Anson, C. Benelli, R. Sessoli and A. K. Powell, *Angew. Chem. Int. Ed.*, **2006**, *45*, 1729.
- ⁵ (a) M. M. Olmstead, A. de Bettencourt-Dias, J. C. Duchamp, S. Stevenson, H. C. Dorn and A. L. Balch, *J. Am. Chem. Soc.* **2000**, *122*, 12220. (b) L. Dunsch, M. Krause, J. Noack and P. Georgi, *J. Phys. Chem. Solids*, **2004**, *65*, 309. (c) S. F. Yang, M. Kalbac, A. Popov and L. Dunsch, *ChemPhysChem*, **2006**, 71990. (d) S. F. Yang, A. A. Popov, M. Kalbac and L. Dunsch, *Chem. Eur. J.*, **2008**, *14*, 2084. (e) S. Yang, A. A. Popov, C. Chen and L. Dunsch, *J. Phys. Chem. C* **2009**, *113*, 7616. (f) S. Stevenson, C. Chancellor, H. M. Lee, M. H. Olmstead and A. L. Balch, *Inorg. Chem.* **2008**, *47*, 1420.
- ⁶ R. Westerström, J. Dreiser, C. Piamonteze, M. Muntwiler, S. Weyeneth, H. Brune, S. Rusponi, F. Nolting, A. Popov, S. Yang, L. Dunsch and T. Greber, *J. Am. Chem. Soc.* **2012**, *134*, 9840.
- ⁷ (a) N. Ishikawa, M. Sugita and W. Wernsdorfer, *Angew. Chem. Int. Ed.* **2005**, *44*, 2931-2935. (b) N. Ishikawa, M. Sugita and W. Wernsdorfer, *J. Am. Chem. Soc.* **2005**, *127*, 3650. (c) N. Ishikawa *Struct. Bonding* **2010**, *135*, 211-228.
- ⁸ (a) G. Christou, D. Gatteschi, D. N. Hendrickson, R. Sessoli, *MRS Bull.* **2000**, *25*, 66-71. (b) D. Gatteschi, R. Sessoli, *Angew. Chem. Int. Ed.* **2003**, *42*, 268-297. (c) M. Murugesu, M. Habrych, W. Wernsdorfer, K. A. Abboud, G. Christou, *J. Am. Chem. Soc.* **2004**, *126*, 4766-4767. (d) A. J. Tasiopoulos, A. Vinslava, W. Wernsdorfer, K. A. Abboud, G. Christou, *Angew. Chem.* **2004**, *116*, 2169-2173. (e) G. Aromi, E. K. Brechin, *Struct. Bonding* **2006**, *122*, 1-67.
- ⁹ A. Caneschi, D. Gatteschi, R. Sessoli, A. L. Barra, L. C. Brunel, M. Guillot, *J. Am. Chem. Soc.* **1991**, *113*, 5873-5874.
- ¹⁰ K. R. Dunbar, *Inorg. Chem.* **2012**, *51*, 12055-12058.
- ¹¹ J.-P. Costes, F. Dahan, W. Wernsdorfer, *Inorg. Chem.* **2006**, *45*, 5-7.
- ¹² (a) R. Sessoli, D. Gatteschi, A. Caneschi, M. Novak, *Nature* **1993**, *365*, 141. (b) Michael N. Leuenberger and D. Loss, *Nature* **2001**, *410*, 789. (c) L. Bogani and W. Wernsdorfer *Nat. Mater.* **2008**, *7*, 179.
- ¹² Tian Huang Jin Zhao Min Feng Alexey A. Popov Shangfeng Yang Lothar Dunsch Hrvoje Petek *Chem. Phys. Lett.* **2012**, *552*, 1.
- ¹³ Tian Huang Jin Zhao Min Feng Alexey A. Popov Shangfeng Yang Lothar Dunsch Hrvoje Petek *Chem. Phys. Lett.* **552**, 1 (2012).
- ¹⁴ Cotton, F. A.; Wilkinson, G. *Advanced Inorganic Chemistry*, 5th edn., John Wiley, New York, **1988**, pp. 776, 955.
- ¹⁵ (a) De Cian, A.; Moussavi, M.; Fischer, J.; Weiss, R. *Inorg. Chem.* **1985**, *24*, 3162. (b) Moussavi, M.; De Cian, A.; Fischer, J.; Weiss, R. *Inorg. Chem.* **1988**, *27*, 1287.
- ¹⁶ (a) Rajaraman, G.; Totti, F.; Bencini, A.; Caneschi, A.; Sessoli, R.; Gatteschi, D. *Dalton Trans.* **2009**, 3153-3161. (b) Singh, S. K.; Tibrewal, N. K.; Rajaraman, G. *Dalton Trans.* **2011**, *40*, 10897-10906.
- ¹⁷ (a) Nakano, H.; Nakayama, K.; Hirao, K.; Dupuis, M. *J. Chem. Phys.* **1997**, *106*, 4912-4917. (b) Roos, B.O.; Andersson, K.; Fulcher, M.K.; Malmqvist, P.-A.; Serrano-Andres, L.; Pierloot, K.; Merchan, M. *Adv. Chem. Phys.* **1996**, *93*, 219-331. (c) Pierloot, K. in Cundari, T. (Ed.). *Computational Organometallic Chemistry*. Marcel Dekker Inc. New York, **2001**, p.123-158.
- ¹⁸ (a) M. Ferbinteanu, F. Cimpoesu, M. A. Gîrtu, C. Enachescu, S. Tanase, *Inorg. Chem.* **2012**, *51*, 40-50. (b) F. Cimpoesu, S. Dahan, S. Ladeira, M. Ferbinteanu, J.-P- Costes, *Inorg. Chem.* **2012**, *51*, 11279-11293.
- ¹⁹ B. G. Wybourne, *Spectroscopic Properties of Rare Earths*, Wiley Interscience, New York, **1965**.
- ²⁰ K.W. H. Stevens, *Proc. Phys. Soc. A* **1952**, *65*,209-215.
- ²¹ Newman, D. J.; Ng, B. K. C. *Crystal Field Handbook*, Cambridge University Press, Cambridge, **2000**.

- ²² (a) B.N. Figgis and M.A. Hitchman, *Ligand Field Theory and its Applications* (Wiley-VCH, New York, **2000**). (b) E.I. Solomon and A.B.P. Lever, editors, *Inorganic Electronic Structure and Spectroscopy* (Wiley & Sons, New York, **1999**).
- ²³ (a) S. Hüfner, *Optical Spectra of Transparent Rare Earth Compounds.*, Academic Press, New York, **1978**. (b) D. J. Newman and B. Ng, *Crystal Field Handbook*, Cambridge University Press, Cambridge, **2000**.
- ²⁴ (a) C. F. Schäffer, *Proc. Roy Soc. A*, **1967**, 297, 96. (b) C. F. Schäffer, *Theoret. Chim. Acta*, **1966**, 4, 166.
- ²⁵ F. Cimpoesu, N. Dragoe, H. Ramanantoanina, W. Urland, and C. Daul, *Phys. Chem. Chem. Phys.* **2014**, 16, 11337.
- ²⁶ W. Fu, J. Zhang, T. Fuhrer, H. Champion, K. Furukawa, T. Kato, J.E. Mahaney, B.G. Burke, K.A. Williams, K. Walker, C. Dixon, J. Ge, C. Shu, K. Harich, and H.C. Dorn, *J. Am. Chem. Soc.* **2011**, 133, 9741.
- ²⁷ (a) L. Noodleman and J.G. Norman, *J. Chem. Phys.* **1979**, 70, 4903. (b) L. Noodleman, *J. Chem. Phys.* **1981**, 74, 5737. (c) A. Bencini and F. Totti, *Int. J. Quant. Chem.* **2005**, 101, 819. (d) M. Mitani, V. Mori, Y. Takano, D. Yamaki, Y. Yoshioka, and K. Yamaguchi, *Chem. Phys.* **2000**, 113, 4035.
- ²⁸ B. Frecus, C.I. Oprea, P. Panait, M. Ferbinteanu, F. Cimpoesu, M. A. Girtu, *Theor. Chem. Acc.* **2014**, 133, 1470
- ²⁹ F. Cimpoesu, B. Frecus, C. I. Oprea, P. Panait, M. A. Girtu, *Comput. Mat. Science* **2014**, 91, 320–328
- ³⁰ M. Ferbinteanu, F. Cimpoesu, and S. Tanase, *Structure and Bonding*, **163**, (2015), pp 185-229.
- ³¹ Hohenberg P, Kohn W. *Phys Rev B* **1964**, 136, 864
- ³² Kohn W, Sham LJ *Phys Rev A* **1965**, 140, 1133.
- ³³ (a) Leininger T, Stoll H, Werner H-J, Savin A *Chem Phys Lett* **1997**, 275, 151. (b) Kohn W, Meir Y, Makarov DE *Phys Rev Lett* **1998**, 80, 4153. (c) Mourik TV, Gdanitz RJ *J Chem Phys* **2002**, 116, 9620.
- ³⁴ Andersson Y, Langreth DC, Lundqvist BI *Phys Rev Lett* **1996**, 76, 102.
- ³⁵ Goll E, Werner HJ, Stoll H, Leininger T, Gori-Giorgi P, Savin A *Chem Phys* **2006**, 329, 276.
- ³⁶ Iikura H, Tsuneda T, Yanai T, Hirao K *J Chem Phys* **2002**, 115, 3540.
- ³⁷ (a) Kamiya M, Tsuneda T, Hirao K *J Chem Phys* **2002**, 117, 6010. (b) Sato T, Tsuneda T, Hirao K *Mol Phys* **2005**, 103, 1151.
- ³⁸ Grimme S, Ehrlich S, Goerigk L *J Comput Chem* **2011**, 32, 1456.
- ³⁹ E. Clar, *Polycyclic Hydrocarbons*, Academic Press, London, **1964**.
- ⁴⁰ Y. Geerts, G. Klärner, K. Müllen, In *Electronic Materials: The Oligomer Approach*, K. Müllen, G. Wagner, Eds.; Wiley-VCH: Weinheim, Germany, **1998**; p 48.
- ⁴¹ C. Joachim and M. A. Ratner, *Proc. Nat. acad. Sci. (US)* **2005**, 102, 8801-8808.
- ⁴² Kahn O., *Molecular Magnetism*, **1993**, VCH Publisher, New York.
- ⁴³ Payne, M.M.; Parkin, S.R.; Anthony, J.E. *J. Am. Chem. Soc.*, **2005**, 127, 8028–8029.
- ⁴⁴ Reddy, A.R.; Bendikov, M. *Chem. Commun.*, **2006**, 1179–1181.
- ⁴⁵ Schön, J.H.; Kloc, C.; Dodabalapur, A.; Batlogg, B. *Science*, **2000**, 289, 599–601.
- ⁴⁶ Raghun, C.; Pati, Y.A.; Ramasesha, S. *Phys. Rev. B*, **2002**, 65, 155204.
- ⁴⁷ Kivelson S.; Chapman, O.L. *Phys. Rev. B*, **1983**, 28, 7236-43.
- ⁴⁸ (a) Philpott, M.R.; Cimpoesu, F., Kawazoe, Y., *Mater Trans*, **2008**, 49(11), 2448 - 2456. (b) Philpott, M.R.; Cimpoesu, F.; Kawazoe, Y., *Chem Phys*, **2008**, 354, 1-15. (c) Pople, J.A.; Walmsley, S.H., *Mol Phys*, **1962**, 5, 15-20.
- ⁴⁹ (a) Higuchi, J., *J. Chem. Phys.*, **1963**, 38, 1237. (b) Longuet-Higgins, H.C., *J. Chem. Phys.* **1950**, 18, 265. (c) Ovchinnikov, A. A; *Theor. Chem. Acc.*, **1978**, 47, 297-304. (d) Lieb, E.H., *Phys Rev Lett*, **1989**, 62, 1201-1204.
- ⁵⁰ (a) Sanvito, S., *Nat Nanotech*, **2007**, 2, 204-206. (b) Pramanik, S.; Stefanita, C.G.; Patibandla, S.; Bandyopadhyay, S.; Garre, K.; Harth, N.; Cahay, M., *Nat Nanotech*, **2007**, 2, 216-219. (c) Dediu, V.A.; Hueso, L.E.; Bergenti, I.; Taliani, C., *Nature Materials*, **2009**, 8, 707-716.
- ⁵¹ (a) Stein, S.E.; Brown, R.L.; *J. Am. Chem. Soc.* **1987**, 109, 3721–3729. (b) Fernandez-Rossier, J.; Palacios, J.J., *Phys. Rev. Lett.* **2007**, 99, 177204-4.
- ⁵² (a) Geim, A.K.; MacDonald, A.H., *Phys Today*, **2007**, 60, 35-41. (b) Novoselov, K.S.; Jiang, D.; Schedlin, F.; Khotkevich, V.V.; Morozov, S.V.; Geim, A.K., *Proc Nat Acad Sci USA*, **2005**, 102, 10451-53.
- ⁵³ Goto, K.; Kubo, T.; Yamamoto, K.; Nakasuji, K.; Sato, K.; Shiomi, D.; Takui, T.; Kubota, M.; Kobayashi, T.; Yakusi, K.; Ouyang, J., *J Am Chem Soc*, **1999**, 121, 1619–1620.
- ⁵⁴ (a) Hicks, R.G., *Org Biomol Chem*, **2007**, 5, 1321–1338. (b) Morita, Y.; Suzuki, S.; Sato, K.; Takui, T., *Nature Chem*, **2011**, 3, 197.
- ⁵⁵ (a) Allinson, G.; Bushby, R. J.; Paillaud, J. L.; Oduwole, D.; Sales, K., *J. Am. Chem. Soc.*, **1993**, 115, 2062-2064. (b) Allinson, G.; Bushby, R.J.; Jesudason, M.V.; Paillaud, J.L.; Taylor, N., *J Chem Soc Perkin Trans*, **1997**, 2, 147-156.

-
- ⁵⁶ Inoue, J.; Fukui, K.; Kubo, T.; Nakazawa, S.; Sato, K.; Shiomi, D.; Morita, Y.; Yamamoto, K.; Takui, T.; Nakasuji, K., *J Am Chem Soc*, **2001**, *123*, 12702–12703.
- ⁵⁷ (a) Li, J.; Duke, B.; McWeeny, R., VB2000 Version 2.0, **2007**, SciNet Technologies, San Diego, CA. (b) Li, J.; McWeeny, R., *Int J Quantum Chem*, **2002**, *89*, 208-216.
- ⁵⁸ Glendening ED, Reed AE, Carpenter JE, Weinhold F, The NBO3.0 program, University of Wisconsin, Copyright 1996-2001
- ⁵⁹ (a) Glendening ED, Weinhold F. *J Comput. Chem.* **1998**, *19*(6), 593-609. (b) Glendening ED, Weinhold F *J Comput. Chem.* **1998**, *19*:610-627. (c) Glendening ED, Badenhoop JK, Weinhold F *J Comput. Chem.* **1998**, *19*, 628-646.
- ⁶⁰ Goto K, Kubo T, Yamamoto K, Nakasuji K, Sato K, Shiomi D, Takui T, Kubota M, Kobayashi T, Yakusi K, Ouyang J *J Am Chem Soc* **1999**, *121*, 1619–1620.